electronics

MDPI

Article

A New MSCSA Technique for Induction Motor Diagnosis Based on the Park Transform Approach

Vitor Fernão Pires [1,2], Paulo Salatiel [1], Armando Cordeiro [2,3], Daniel Foito [1,4], Armando J. Pires [1,4,*] and João F. A. Martins [4,5]

1 Escola Superior de Tecnologia de Setúbal (EST Setubal), Instituto Politécnico de Setúbal, 2914-508 Setúbal, Portugal; vitor.pires@estsetubal.ips.pt (V.F.P.); pcmsalatiel@gmail.com (P.S.); daniel.foito@estsetubal.ips.pt (D.F.)
2 Investigation and Development Center, Institute for Systems and Computer Engineering: Research and Development in Lisbon (INESC-ID), 1000-029 Lisboa, Portugal; armando.cordeiro@isel.pt
3 Instituto Superior de Engenharia de Lisboa (ISEL), Lisboa Polytechnic University, 1959-007 Lisboa, Portugal
4 CTS-UNINOVA, LASI, 2829-517 Caparica, Portugal; jf.martins@fct.unl.pt
5 NOVA School of Science and Technology, NOVA University Lisbon (UNL), 2829-516 Caparica, Portugal
* Correspondence: armando.pires@estsetubal.ips.pt

Abstract

Induction machines play a crucial role in industrial applications, making preventive maintenance combined with fault diagnosis techniques essential for ensuring reliable operation. One of the most widely used diagnostic methods for induction machines is Motor Current Signature Analysis (MCSA). However, this technique has certain limitations, particularly in the detection of incipient or small faults. Another well-established technique is Motor Square Current Signature Analysis (MSCSA), which overcomes some of the limitations of MCSA by extracting additional fault-related information from the motor current signals. This paper proposes a new diagnostic technique, designated MSCSA-APT (Motor Square Current Signature Analysis–Alternative Park Transform), based on the spectral analysis of motor currents. Compared with the conventional MSCSA method, the proposed approach provides additional information from the frequency-domain analysis, thereby improving fault detection capability. The method is based on the square of the motor square current signal and employs an Alternative Park Transform (APT) to enhance the extraction of fault signatures. Simulation and experimental results are presented to validate the proposed approach. Although the method has been evaluated for the identification of different types of faults, it is particularly effective in detecting stator short-circuit faults.

Keywords: induction motor; diagnosis; fault detection; stator currents; MCSA; MSCSA; MSCSA-APT; alternative park transform

Academic Editor: Zhongyong Zhao

Received: 14 June 2026
Revised: 20 July 2026
Accepted: 23 July 2026
Published: 28 July 2026

1. Introduction

Induction machines are widely used in industrial applications because their reliability and service continuity are essential requirements in modern industry. To ensure these requirements are met, preventive maintenance programs incorporating fault diagnosis techniques are indispensable. Induction machines are susceptible to various types of faults, including stator electrical faults, rotor electrical faults, and mechanical faults. To detect and diagnose these faults, numerous condition monitoring methods have been proposed, enabling the identification of anomalies in one or more operating characteristics of the machine.

 https://doi.org/10.3390/electronics15153323

Many fault diagnosis methods for electrical machines, based on different measured signals, have been developed in recent years [1–6]. Among the most common approaches are electromagnetic field monitoring, temperature measurement, infrared thermography, radio-frequency emission monitoring, acoustic noise analysis, vibration monitoring, and stator current signature analysis (MCSA) [7–9]. In these methods, the presence of a fault is identified through specific features extracted from the corresponding sensor signals. Among the various diagnostic signatures, the stator current remains one of the most widely used due to its non-invasive nature, ease of measurement, and proven effectiveness in fault detection and diagnosis.

Numerous fault diagnosis methods based on induction motor line currents have been proposed [10–13]. One of the most widely adopted techniques is Motor Current Signature Analysis (MCSA), which identifies characteristic sideband components around the supply frequency [14–16]. More advanced signal-processing techniques, including wavelet transforms, the Hilbert Transform, the Hilbert–Huang Transform, and time-series data mining, have also been proposed [17–20]. In addition, other methods extract fault-related features from the stator current, such as those based on the Park's Vector approach [21] and various pattern recognition techniques [22,23]. More recently, advances in digital technology have enabled the application of artificial intelligence techniques, including neural networks, fuzzy logic, and expert systems [24–27]. However, many of these intelligent methods require prior knowledge of the system for training or parameter tuning. A common characteristic of all the aforementioned methods is that they rely exclusively on the induction motor stator current. Consequently, their diagnostic performance ultimately depends on the amount and quality of the information contained in the measured current signal. Enriching the information content of this signal can therefore improve the effectiveness of both conventional and advanced diagnostic techniques. To this end, alternative representations of the stator current have been proposed, including the Current Space Vector and the Park's Vector [28,29]. Other approaches combine the stator current with the supply voltage to obtain additional diagnostic information. Among these, the instantaneous power method has been widely used for fault detection [30–32], as it provides more comprehensive fault-related information than the current signal alone. However, this technique requires two separate sensors to measure both electrical quantities. To overcome this limitation, alternative methods have been proposed. One such technique employs the square of the stator current instead of combining current and voltage measurements [33]. Designated as Motor Square Current Signature Analysis (MSCSA), this method extracts additional diagnostic information comparable to that provided by the instantaneous power approach while requiring only current measurements, thereby simplifying the sensing infrastructure. Similarly, the Extended Park's Vector approach [34] provides significantly richer diagnostic information than the classical Park's Vector.

In recent years, the paradigm of induction motor condition monitoring has experienced a significant shift towards Artificial Intelligence (AI) and data-driven architectures. Driven by the availability of high-frequency data from sensors, researchers have extensively deployed deep learning frameworks to handle non-linear and multi-class mechanical and electrical anomalies simultaneously. Convolutional Neural Networks (CNNs) and Long Short-Term Memory (LSTM) networks have emerged as powerful tools, particularly due to their automated feature-extraction capability which bypasses the need for manual spectral-band searching. For instance, hybrid frameworks fusing CNN and LSTM blocks with attention mechanisms have been widely adopted to process time-series vibrational and stator current variables for real-time tracking of broken rotor bars and winding degradation [35–40]. Furthermore, ensemble systems—such as Weighted Probability Ensemble Deep Learning (WPEDL)—have demonstrated remarkable accuracy by incorporating 2D feature maps generated through Short-Time Fourier Transforms (STFT) or Empirical Wavelet Transforms (EWT). More recently, self-attention mechanisms and transformer-based architectures, originally tailored for natural language processing, have been successfully tailored to industrial electrical machine diagnosis. These models capture long-range temporal dependencies and spatial signal cross-modulations far more effectively than classical shallow networks. However, despite their impressive multi-class classification accuracies (often exceeding 98%), deep learning, hybrid, and transformer-based networks carry inherent drawbacks for widespread industrial edge deployment. They function essentially as mathematical 'black-boxes' lacking strict physical explainability, are highly sensitive to data imbalance (often requiring techniques like SMOTE to function reliably under scarce fault data), and impose substantial computational overhead, latency, and memory footprints on industrial edge microcontrollers. It is important to emphasize that while these advanced AI-driven algorithms operate using motor stator currents as their core input, their overall diagnostic accuracy and feature-extraction robustness can be significantly enhanced if the raw current signals are pre-processed or structured using specialized formulations such as Motor Current Signature Analysis (MCSA), the Extended Park Vector Approach, or other vector-based transformation methods.

Within this context, this paper proposes a new method based on the MSCSA technique that enables the extraction of additional fault-related information from the measured motor current. Although the conventional MSCSA method has proven effective for fault diagnosis, its diagnostic capability is limited under certain fault conditions. To address this limitation, the proposed technique enhances fault detection by extracting richer frequency-domain features from the motor current signal. The proposed approach, designated as Motor Square Current Signature Analysis–Alternative Park Transform (MSCSA-APT), is validated through both simulation and experimental results obtained from a laboratory test setup.

2. Detection and Diagnosis Using MCSA and MSCSA Techniques

As discussed previously, one of the most widely used methods for fault detection and diagnosis in induction machines is based on the spectral analysis of the stator current. This technique monitors the stator current while the motor is operating to detect incipient faults, allowing early intervention before partial or complete machine failure occurs. Several diagnostic techniques have been developed based on this principle, the most well-known being Motor Current Signature Analysis (MCSA). A more recent technique, derived from the instantaneous power method but requiring only a single current sensor, is Motor Square Current Signature Analysis (MSCSA). This method has demonstrated superior diagnostic performance by extracting more fault-related information from the motor current signal than conventional MCSA.

2.1. MCSA Technique

The MCSA technique is non-invasive and relatively simple, as it requires the acquisition of the current signal from only one stator phase. A spectral analysis of the acquired current signal is then performed to detect, identify, and assess the severity of faults in the induction machine [14–16].

In its simplest form, a stator current monitoring system based on the MCSA technique is illustrated in Figure 1. As can be seen, the monitoring system consists of a current transformer, a signal acquisition system, and a data processing unit that computes the frequency spectrum used for fault diagnosis.

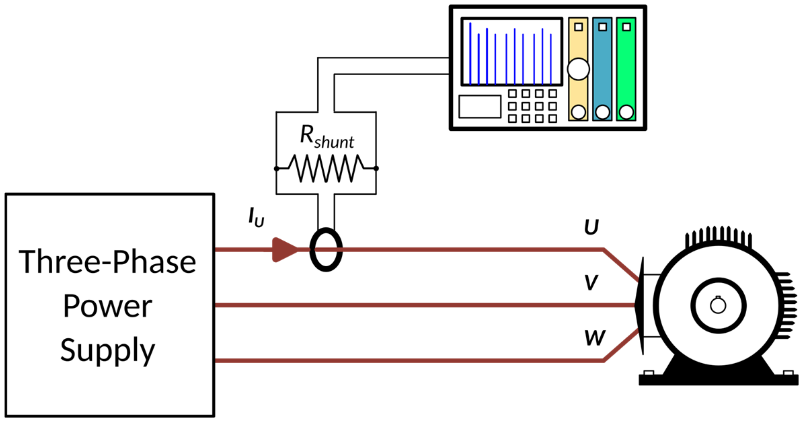

Figure 1. Stator Electric Current Monitoring System in its Basic Version.

While the classical MCSA and MSCSA techniques mathematically require only a single-phase current sensor to extract fault signatures, practical 24/7 industrial deployments typically utilize multi-phase measurements to ensure hardware redundancy, fault tolerance, and protection against sensor signal loss during continuous operation.

Assuming ideal operating conditions for both the induction motor and the power supply, the phase current can be expressed as (1).

$$i_M(t) = I_{max}\sin(\omega t - \alpha) \quad (1)$$

where I_{max} is the maximum amplitude of the current, ω the angular frequency and α the phase angle.

From this equation, it is clear that the phase current spectrum contains only the fundamental frequency component, f = ω/2π, as can be seen in Figure 2.

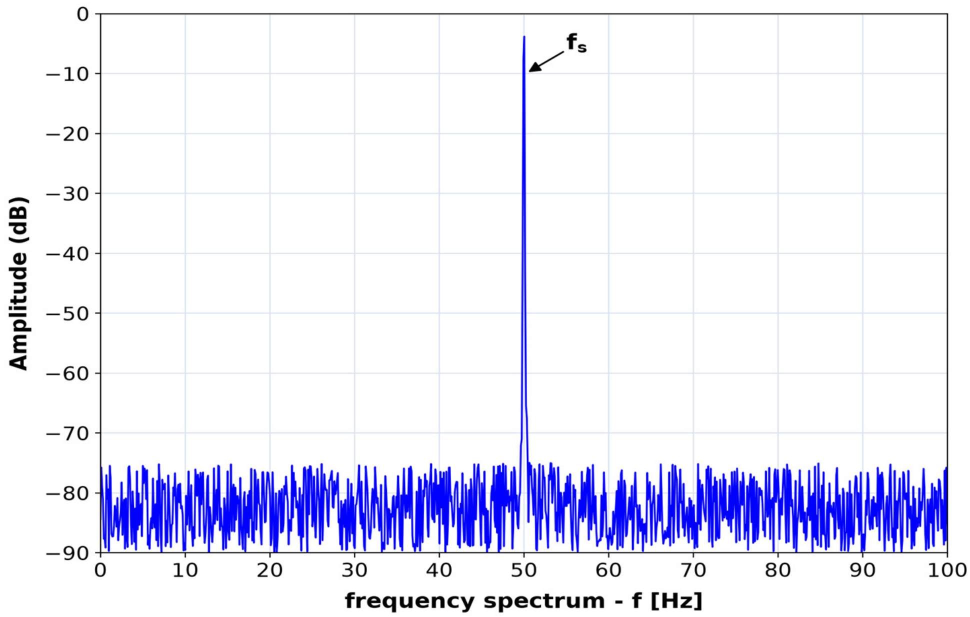

Figure 2. Frequency spectrum of the stator current for a healthy motor—MCSA technique.

However, when a fault occurs in the motor, the presence of only the fundamental frequency component is no longer valid. Additional frequency components appear in the current spectrum, and these can be used to detect and diagnose motor faults. One of the most common faults affecting induction machines is the stator winding fault. Stator winding faults can occur in several forms; however, inter-turn short circuits within the same coil or short circuits between coils of the same phase group are generally considered the initial stage of more severe stator winding failures [3].

According to [41], the voltage between adjacent turns of a stator coil typically ranges from 10 to 100 V, while the insulation separating these turns is only about 0.5 mm thick. Consequently, switching operations, motor start-up, or sudden load changes may generate transient overvoltages that gradually degrade the turn-to-turn insulation. In most cases, stator faults in induction machines result from multiple short circuits within the windings of the same phase, caused by the partial or complete breakdown of the insulation between adjacent turns.

When an inter-turn short circuit occurs, the maximum value of the line current in the affected phase increases relative to the currents in the other phases. In addition, the phase displacement between the stator currents deviates from the ideal value of 120°. However, for the sake of simplicity, it is assumed that the short-circuited phase exhibits a different current amplitude while the phase displacement between the three stator currents remains equal to 120°. This assumption simplifies the analytical development without affecting the validity of the proposed method. An inter-turn short circuit produces a high thermal gradient in the faulted region and generates a circulating current in the damaged winding. As a result, a reverse rotating magnetic field is produced, giving rise to an inverse magnetomotive force (MMF) that reduces the average MMF generated by the induction machine. Consequently, the air-gap magnetic flux becomes asymmetric, leading to the appearance of additional frequency components associated with the stator fault. These frequency components depend on the motor characteristics and can be determined using (2).

$$f_s = \left\{ \frac{n}{pp}(1-s) \pm k \right\} f \tag{2}$$

where f_S is the additional frequency components that appear in the current signal in the event of a stator short-circuit, n is a natural number, pp the number of pole pairs, s the slip, k the harmonic order and f the grid fundamental frequency.

The spectrum of the phase current resulting from this type of fault is shown in Figure 3. As can also be observed in this figure, the amplitudes of the additional frequency components increase as the fault severity increases.

2.2. MSCSA Technique

The MCSA technique has significantly advanced induction motor fault diagnosis because it is completely non-invasive and requires only a single current sensor to acquire the stator current signal [33]. More recently, another technique, known as Motor Square Current Signature Analysis (MSCSA), has been proposed. Like MCSA, it requires only one current sensor but is capable of extracting additional fault-related information from the motor current signal. The application of the MSCSA technique can be divided into the following three steps:

- Acquiring one stator phase current;
- Performing the square of the acquired current;
- Computing the frequency analysis of the square current.

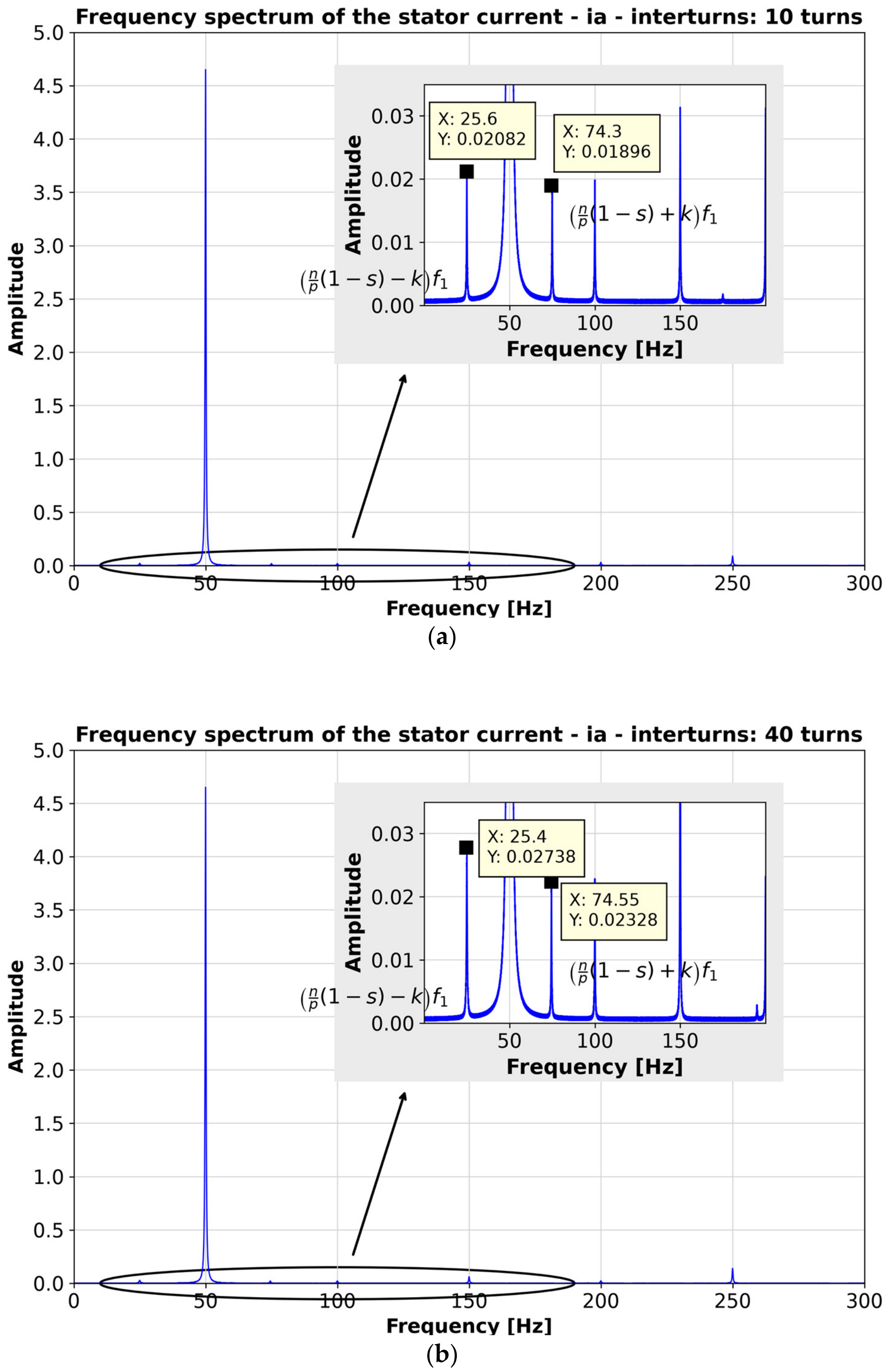

Figure 3. Frequency spectrum of the stator current—stator short-circuit—(**a**) 10 turns, (**b**) 40 turns—MCSA technique.

Since this technique performs spectral analysis on the square of the stator current, even under healthy operating conditions with a balanced sinusoidal supply voltage, the resulting spectrum contains more than one frequency component. Specifically, it consists of a DC component and a fundamental component at twice the supply frequency, (f_S = 2ω/2π), as expressed by (3) and Figure 4.

$$i_M^2(t) = \frac{I_{max}^2}{2} + \frac{I_{max}^2}{2}\sin\left(2\omega t - 2\alpha - \frac{\pi}{2}\right) \quad (3)$$

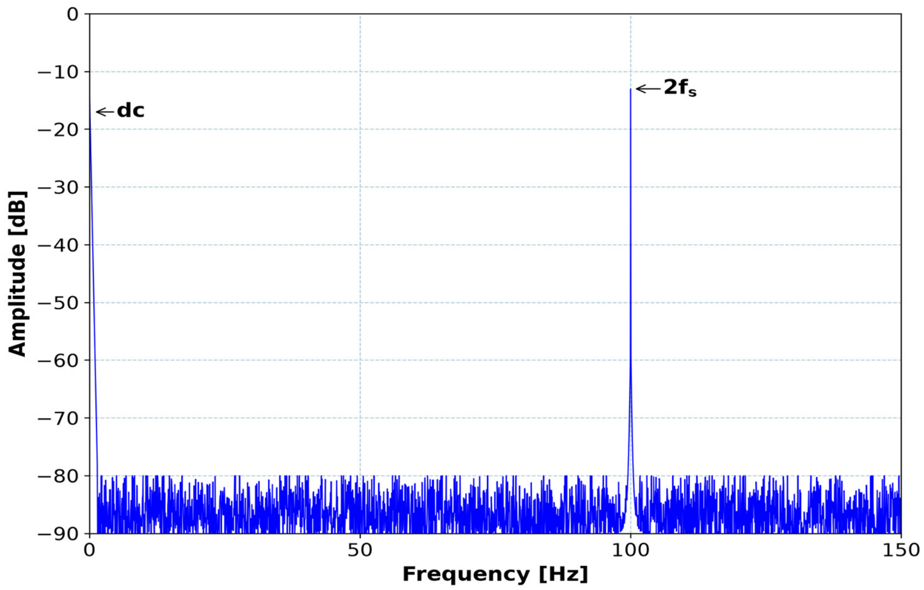

Figure 4. Frequency spectrum of the square stator current for a healthy motor—MSCSA technique.

The MSCSA technique is now applied to the case of stator inter-turn short circuits. In this section, the resulting frequency spectra and the corresponding expression for calculating the fault severity index are analyzed. Compared with the conventional MCSA technique, MSCSA offers the advantage of a richer spectral content, characterized by a larger number of fault-related sideband components. However, for this type of fault, the relationship between the fault severity index and the percentage of short-circuited turns is relatively weak, resulting in limited sensitivity for assessing fault severity.

When the induction machine operates with an inter-turn short circuit, the stator current can be represented by (4).

$$i_M(t) = I_{max}\sin(\omega t - \alpha) + I_{max\_lo}\sin\left[\left(\frac{n}{pp}(1-s) - k\right)\omega t - \beta_{lo}\right] + I_{max\_up}\sin\left[\left(\frac{n}{pp}(1-s) + k\right)\omega t - \beta_{up}\right] \quad (4)$$

where I_{max}, I_{max_lo} and I_{max_up} correspond to the maximum value of the current of the fundamental component, lower sideband and upper sideband, respectively.

By squaring (4), a signal composed of ten terms is obtained, as expressed in (5).

$$\begin{aligned}
i_M^2(t) = {} & \left(\tfrac{I_{max_sc}^2 + I_{max_lo_sc}^2 + I_{max_up_sc}^2}{2}\right) + \tfrac{I_{max_sc}^2}{2}\sin\left(2\omega t - 2\alpha + \tfrac{\pi}{2}\right) \\
& + \left(I_{max_lo_sc} \cdot I_{max_up_sc}\right)\sin\left(2k\omega t + \beta_{lo} - \beta_{up} - \tfrac{\pi}{2}\right) \\
& + \left(I_{max_lo_sc} \cdot I_{max_up_sc}\right)\sin\left(\tfrac{2n}{pp}(1-s)\omega t - \beta_{lo} - \beta_{up} + \tfrac{\pi}{2}\right) \\
& + \left(\tfrac{I_{max_lo_sc}^2}{2}\right)\sin\left[\left(\tfrac{2n}{pp}(1-s) - 2k\right)\omega t - 2\beta_{lo} + \tfrac{\pi}{2}\right] \\
& + \left(\tfrac{I_{max_up_sc}^2}{2}\right)\sin\left[\left(\tfrac{2n}{pp}(1-s) + 2k\right)\omega t - 2\beta_{up} + \tfrac{\pi}{2}\right] \\
& + \left(I_{max_sc} \cdot I_{max_lo_sc}\right)\sin\left[\left(\tfrac{n}{pp}(1-s) + 1 - k\right)\omega t + \sigma - \beta_{lo} - \tfrac{\pi}{2}\right] \\
& + \left(I_{max_sc} \cdot I_{max_up_sc}\right)\sin\left[\left(\tfrac{n}{pp}(1-s) + 1 + k\right)\omega t + \sigma - \beta_{up} - \tfrac{\pi}{2}\right] \\
& + \left(I_{max_sc} \cdot I_{max_lo_sc}\right)\sin\left[\left(\tfrac{n}{pp}(1-s) - 1 - k\right)\omega t - \sigma + \beta_{lo} + \tfrac{\pi}{2}\right] \\
& + \left(I_{max_sc} \cdot I_{max_up_sc}\right)\sin\left[\left(\tfrac{n}{pp}(1-s) - 1 + k\right)\omega t - \sigma + \beta_{up} + \tfrac{\pi}{2}\right]
\end{aligned} \quad (5)$$

The first and second terms of (5) correspond to the DC component and the fundamental frequency component of the signal, respectively, which are present under all operating conditions. In the presence of inter-turn short circuits, additional frequency components appear that are distinct from those associated with other types of faults. For the analysis of these additional frequency components, the parameters (k = 1), (n = 1), and (pp = 2) are considered. It is also assumed that the induction machine operates from a 50 Hz supply with a slip of up to 5%. Under these assumptions, it follows that:

- The third term of (5) contributes a frequency component at ($2kf$). Under the assumptions defined above, this corresponds to the fundamental component at 100 Hz. For other values of (k), this term gives rise to frequency components at different frequencies.
- The fourth term of the signal will contribute with a component that will be inserted in $\left(\frac{2n}{pp}(1-s)\right)f$, so this frequency component will appear between 47.5 Hz and 50 Hz, exclusive.
- The fifth and sixth terms of the signal represent sidebands around the $2f$ fundamental component, as they will appear, in the respective frequency spectrum, at $\left(\frac{2n}{pp}(1-s)-2k\right)f$. In the case of the fifth term, this will take place between 50 Hz and 52.5 Hz, inclusive, and the sixth term will take place between 147.5 Hz and 150 Hz, exclusive.
- The seventh and tenth terms of the signal, under the conditions presented above, will eventually contribute to the same additional frequency component, located at $\left(\frac{n}{pp}(1-s)\right)f$. This frequency will be between 23.75 Hz and 25 Hz.
- In relation to the eighth and ninth terms, as in the case of the fifth and sixth terms, these represent sidebands around the fundamental component, as they will appear in $\left(\frac{n}{pp}(1-s)+1+k\right)f$ and $\left(\frac{n}{pp}(1-s)-1-k\right)f$. These will appear between 123.75 Hz and 125 Hz, exclusive and 75 Hz and 76.25 Hz, inclusive, respectively.

It can therefore be concluded that, in the case of stator inter-turn short-circuit faults, the MSCSA technique produces characteristic frequency components that enable reliable and effective fault detection. The presence of these frequency components can be used to determine whether an induction machine is operating under stator inter-turn short-circuit conditions. To illustrate these characteristics, the frequency spectrum of the squared stator current signal under stator inter-turn short-circuit conditions is shown in Figure 5.

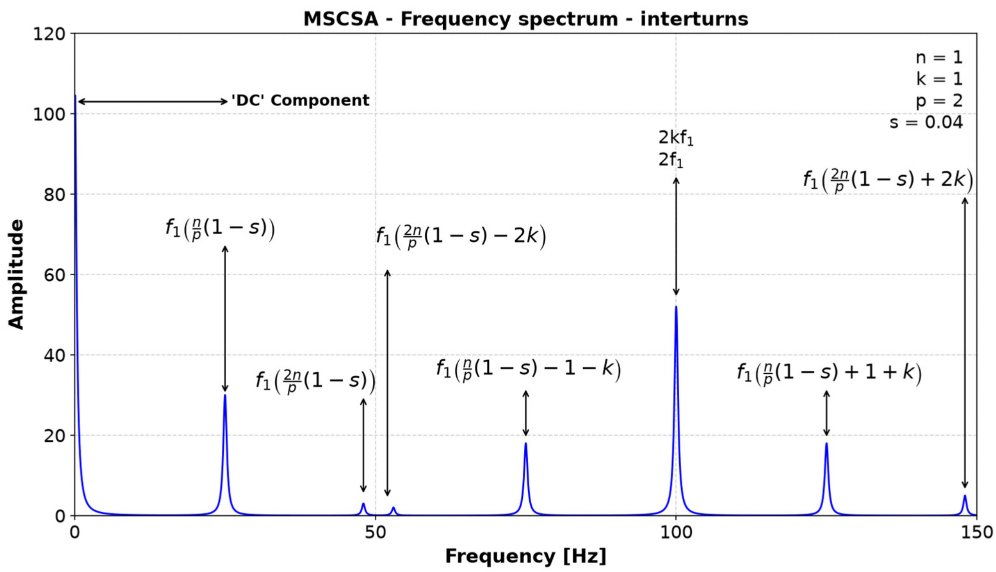

Figure 5. Frequency spectrum of the stator current square–stator short-circuit—MSCSA technique (simulation result).

Considering that the fundamental component of the signal obtained using the MSCSA technique is located at (2f), and that the dominant fault-related frequency component for stator inter-turn short-circuit faults appears at ($\frac{n}{pp}(1-s)f$), the fault severity index can be defined by (6). This index is used to evaluate the severity of the fault and to compare the performance of the proposed diagnostic technique, as discussed in Section 3.

$$SF_{MSCSA\_sc} = \frac{\left| i^2_{a\_sc}\left\{ \left(\frac{n}{pp}(1-s) \right) f \right\} \right|}{\left| i^2_{a\_sc}\{2f\} \right|} \tag{6}$$

3. Detection and Diagnosis Using MSCSA-APT Techniques

In the previous section, the MSCSA technique was briefly introduced. This method performs fault detection and diagnosis based on the spectral analysis of the squared stator current signal. Compared with the conventional MCSA technique, MSCSA offers several advantages, including a richer spectral content and a higher fault severity index, particularly for stator inter-turn short-circuit faults. However, an important question arises: is it possible to extract even more diagnostic information, thereby further increasing the fault severity index and improving fault sensitivity? To address this question, this paper proposes a new method based on the MSCSA technique. The proposed approach, designated as Motor Square Current Signature Analysis–Alternative Park Transform (MSCSA-APT), employs a modified version of the Park transform. The proposed fault diagnosis technique is based on the spectral analysis of the squared quadrature-axis current component in the Alternative Park reference frame. Since this quadrature-axis component is itself obtained from the squared stator current signal, the resulting analysis is effectively performed on the square of the squared current signal, providing additional fault-related information.

The Park transform applied to the stator currents is obtained by multiplying the current vector in the (alpha/beta) reference frame by the well-known Park transformation matrix, as given in (7).

$$P = \begin{bmatrix} \cos\theta & \sin\theta & 0 \\ -\sin\theta & \cos\theta & 0 \\ 0 & 0 & 1 \end{bmatrix} \tag{7}$$

where θ represents the position of the frame associated with the transformation.

Following the principle underlying the Park transform, the sine and cosine terms can be replaced by expressions associated with the alpha- and beta-axis currents. Accordingly, the cosine terms are replaced by ($-i_\beta$), while the sine terms are replaced by (i_α).

As a result, the conventional Park transformation matrix is reformulated, giving rise to the modified matrix (P'), as defined in (8). The corresponding expression for the stator currents in the ($dq0'$) reference frame is then given by (9).

$$P' = \begin{bmatrix} -i_\beta & i_\alpha & 0 \\ -i_\alpha & -i_\beta & 0 \\ 0 & 0 & 1 \end{bmatrix} \tag{8}$$

$$\begin{bmatrix} i'_d \\ i'_q \\ i'_0 \end{bmatrix} = \begin{bmatrix} -i_\beta & i_\alpha & 0 \\ -i_\alpha & -i_\beta & 0 \\ 0 & 0 & 1 \end{bmatrix} \begin{bmatrix} i_\alpha \\ i_\beta \\ i_0 \end{bmatrix} \tag{9}$$

Once the expressions for the stator currents in the (abc) reference frame are established, the proposed Park transformation is applied. After the corresponding mathematical simplifications, the expressions for a healthy induction motor are obtained, as given in (10) and (11).

$$i'_d(t) = 0 \tag{10}$$

$$i'_q(t) = -\frac{3}{2} I_{max}^2 \tag{11}$$

As can be observed from (10) and (11), the expressions for the direct- and quadrature-axis currents obtained using the proposed Park transformation show that the direct-axis current, (i'_d), is always equal to zero. This result holds regardless of whether the induction machine is operating under healthy or faulty conditions, since the corresponding terms always cancel each other. Therefore, only the quadrature-axis current, (i'_q), is considered for the subsequent spectral analysis.

For the healthy operating condition, assuming a balanced three-phase supply voltage, the resulting signal can be expressed by (12). This expression is obtained simply by squaring (11).

$$i'^2_q(t) = \frac{9}{4} I_{max}^4 \tag{12}$$

From (12), it can be seen that the resulting signal is a constant. Therefore, it can be concluded that, for the MSCSA-APT technique, the fundamental component of the signal is located at 0 Hz (DC).

To further clarify the physical meaning and the diagnostic uniqueness of the proposed Alternative Park Transform (APT), it is crucial to analyze its underlying structure in comparison with conventional coordinate transformations. By replacing the traditional trigonometric weights ($cos\theta$ and $sin\theta$) with the orthogonal current components themselves ($-i_\beta$ and i_α), the coordinate frame becomes dynamically bound to the instantaneous orientation of the current space vector.Consequently, by construction, the projection along the direct axis (i'_d) becomes identically zero under all operating conditions (balanced, unbalanced, or faulty) because the transformation matrix forces the frame to remain strictly orthogonal to the space vector (13).

$$i'_d = i_\alpha(-i_\beta) + i_\beta(i_\alpha) = 0 \tag{13}$$

As a result, the entire energy of the space vector collapses onto the quadrature axis (i'_q), where $i'_q = -\left(i_\alpha^2 + i_\beta^2\right) = -\|i\|^2$. Since the MSCSA-APT technique performs spectral analysis on the square of this resulting q-axis current, the final monitored quantity is mathematically expressed as (14).

$$\left(i'_q\right)^2 = \left(i_\alpha^2 + i_\beta^2\right)^2 = \|i\|^4 \tag{14}$$

This formulation reveals that the proposed method mathematically evaluates the fourth power of the current space vector modulus. However, this approach is fundamentally distinct from a conventional single-phase (scalar) fourth-order current analysis (such as analyzing a single line current to the fourth power, i_α^4). While a scalar fourth-order approach generates self-convolution harmonics confined to a single phase, the proposed vector-based implementation cross-modulates the orthogonal α and β variables. Because i_α and i_β intrinsically embed the phase asymmetries and negative-sequence components caused by stator winding faults, their cross-products create a unique matrix of frequency mixing terms that significantly amplify fault visibility while suppressing non-fault-related noise. To contextualize the diagnostic novelty of the MSCSA-APT approach, Table 1 compares its core performance metrics against alternative established methodologies, such as Park's Vector Modulus (PVM), the Extended Park's Vector Approach (EPVA), Instantaneous Power analysis, and standard Motor Square Current Signature Analysis (MSCSA).

Table 1. Comparative analysis of the proposed MSCSA-APT against existing diagnostic methods.

Method	Signal Analysed	Sensing Required	Physical Manifestation/Frequency Shifts
Park's Vector Modulus (PVM)	$\|i\| = \sqrt{i_\alpha^2 + i_\beta^2}$	2 or 3 Current Sensors	Maps spatial asymmetry. Healthy = DC. Faulty = introduces $2f$ oscillations due to negative sequence components. Contains a non-linear square root that squashes harmonic sidebands.
Extended Park's Vector Approach (EPVA)	$\|i\|^2 = i_\alpha^2 + i_\beta^2$	2 or 3 Current Sensors	Analyzes the squared modulus directly to remove the square-root bottleneck. Healthy = DC (0 Hz). Faulty = isolates negative sequence components at $2f$ and fault sidebands.
Instantaneous Power	$p(t) = v_a i_a + v_b i_b + v_c i_c$	Voltage & Current Sensors	Contains information on both supply grid anomalies and machine faults. Healthy = DC. Faulty = oscillations at $2f$ and fault sidebands.
MSCSA	i_a^2	1 Current Sensor Only	Mimics instantaneous power spectral features using only a single scalar sensor. Shifts fundamental component to $2f$. Fault sidebands modulate around $2f$.
Proposed MSCSA-APT	$\left(i_q'\right)^2 = \left(i_\alpha^2 + i_\beta^2\right)^2$	2 or 3 Current Sensors	A true vector-squared squaring technique. It shifts the fundamental component back to 0 Hz (DC) but subjects the fault-induced asymmetry sidebands to an extra stage of frequency cross-modulation.

As outlined in Table 1, the proposed MSCSA-APT offers two distinct practical advantages over the state-of-the-art:

1. Elimination of Supply Frequency Leakage: Unlike standard MSCSA, which shifts the fundamental current component to $2f$ where it can overwhelm subtle adjacent sidebands, MSCSA-APT translates the fundamental component to a constant DC value (0 Hz). This unburdens the active AC spectrum, drastically lowering the noise floor.
2. Multiplication of Fault Signatures: By subjecting the fault-induced asymmetry to a secondary squaring operation ($\|i\|^4$), it creates an expanded array of inter-modulated sidebands. This structural feature significantly increases the Severity Index (SF), rendering the fault detection mechanism highly sensitive and resilient to load variations.

The application of the proposed technique to an induction machine operating with a stator winding fault, namely an inter-turn short circuit, is now analyzed. For this purpose, the analysis starts from the stator current expressions in the ($\alpha\beta$) reference frame under inter-turn short-circuit conditions, as given in (15) and (16).

$$
\begin{aligned}
i_{\alpha\_sc}(t) = {} & \left(\sqrt{\tfrac{1}{6}} I_{max} + \sqrt{\tfrac{2}{3}} I_{max\_sc}\right)\sin(\omega t - \alpha) \\
& + \left(\sqrt{\tfrac{1}{6}} I_{max\_lo} + \sqrt{\tfrac{2}{3}} I_{max\_lo\_sc}\right)\sin\left[\left(\tfrac{n}{pp}(1-s) - k\right)\omega t - \beta_{lo}\right] \\
& + \left(\sqrt{\tfrac{1}{6}} I_{max\_up} + \sqrt{\tfrac{2}{3}} I_{max\_up\_sc}\right)\sin\left[\left(\tfrac{n}{pp}(1-s) + k\right)\omega t - \beta_{up}\right]
\end{aligned} \quad (15)
$$

$$
\begin{aligned}
i_{\beta\_sc}(t) = {} & \left(\sqrt{\tfrac{3}{2}} I_{max}\right) \sin\left(\omega t - \alpha - \tfrac{\pi}{2}\right) \\
& + \left(\sqrt{\tfrac{3}{2}} I_{max\_lo}\right) \sin\left[\left(\tfrac{n}{pp}(1-s) - k\right)\omega t - \beta_{lo} - \tfrac{\pi}{2}\right] \\
& + \left(\sqrt{\tfrac{3}{2}} I_{max\_up}\right) \sin\left[\left(\tfrac{n}{pp}(1-s) + k\right)\omega t - \beta_{up} - \tfrac{\pi}{2}\right]
\end{aligned} \tag{16}
$$

An intermediate step in the derivation is to calculate the sum of the squared current components using the expressions derived previously. Based on this result, the expression for the quadrature-axis current is obtained, as given in (17).

$$
\begin{aligned}
i'_{q\_sc}(t) = {} & -\Big(\tfrac{5}{6} I_{max}^2 + \tfrac{1}{3} I_{max\_sc}^2 + \tfrac{5}{6} I_{max\_lo}^2 + \tfrac{1}{3} I_{max\_lo\_sc}^2 + \tfrac{5}{6} I_{max\_up}^2 + \tfrac{1}{3} I_{max\_up\_sc}^2 + \tfrac{1}{3} I_{max} I_{max\_sc} \\
& + \tfrac{1}{3} I_{max\_lo} I_{max\_lo\_sc} + \tfrac{1}{3} I_{max\_up} I_{max\_up\_sc}\Big) \\
& + \left(\tfrac{1}{3} I_{max\_sc}^2 - \tfrac{2}{3} I_{max}^2 + \tfrac{1}{3} I_{max} I_{max\_sc}\right) \sin\left(2\omega t - 2\alpha + \tfrac{\pi}{2}\right) \\
& + \Big(\tfrac{5}{3} I_{max\_lo} I_{max\_up} + \tfrac{2}{3} I_{max\_lo\_sc} I_{max\_up\_sc} + \tfrac{1}{3} I_{max\_lo} I_{max\_up\_sc} \\
& + \tfrac{1}{3} I_{max\_lo\_sc} I_{max\_up}\Big) \sin\left(2k\omega t + \beta_{lo} - \beta_{up} + \tfrac{3\pi}{2}\right) \\
& + \Big(\tfrac{2}{3} I_{max\_lo\_sc} I_{max\_up\_sc} - \tfrac{4}{3} I_{max\_lo} I_{max\_up} + \tfrac{1}{3} I_{max\_lo} I_{max\_up\_sc} \\
& + \tfrac{1}{3} I_{max\_lo\_sc} I_{max\_up}\Big) \sin\left(\tfrac{2n}{pp}(1-s)\omega t - \beta_{lo} - \beta_{up} + \tfrac{\pi}{2}\right) \\
& + \left(\tfrac{1}{3} I_{max\_lo\_sc}^2 - \tfrac{2}{3} I_{max\_lo}^2 + \tfrac{1}{3} I_{max\_lo} I_{max\_lo\_sc}\right) \sin\left(\left(\tfrac{2n}{pp}(1-s) - 2k\right)\omega t - 2\beta_{lo} + \tfrac{\pi}{2}\right) \\
& + \left(\tfrac{1}{3} I_{max\_up\_sc}^2 - \tfrac{2}{3} I_{max\_up}^2 + \tfrac{1}{3} I_{max\_up} I_{max\_up\_sc}\right) \sin\left(\left(\tfrac{2n}{pp}(1-s) + 2k\right)\omega t - 2\beta_{up} + \tfrac{\pi}{2}\right) \\
& + \Big(\tfrac{2}{3} I_{max\_sc} I_{max\_lo\_sc} - \tfrac{4}{3} I_{max} I_{max\_lo} + \tfrac{1}{3} I_{max} I_{max\_lo\_sc} \\
& + \tfrac{1}{3} I_{max\_sc} I_{max\_lo}\Big) \sin\left(\left(\tfrac{n}{pp}(1-s) + 1 - k\right)\omega t - \alpha - \beta_{lo} + \tfrac{\pi}{2}\right) \\
& + \Big(\tfrac{2}{3} I_{max\_sc} I_{max\_up\_sc} - \tfrac{4}{3} I_{max} I_{max\_up} + \tfrac{1}{3} I_{max} I_{max\_up\_sc} \\
& + \tfrac{1}{3} I_{max\_sc} I_{max\_up}\Big) \sin\left(\left(\tfrac{n}{pp}(1-s) + 1 + k\right)\omega t - \alpha - \beta_{up} + \tfrac{\pi}{2}\right) \\
& + \Big(\tfrac{5}{3} I_{max} I_{max\_lo} + \tfrac{2}{3} I_{max\_sc} I_{max\_lo\_sc} + \tfrac{1}{3} I_{max} I_{max\_lo\_sc} \\
& + \tfrac{1}{3} I_{max\_sc} I_{max\_lo}\Big) \sin\left(\left(\tfrac{n}{pp}(1-s) - 1 - k\right)\omega t - \alpha - \beta_{lo} + \tfrac{\pi}{2}\right) \\
& + \Big(\tfrac{5}{3} I_{max} I_{max\_up} + \tfrac{2}{3} I_{max\_sc} I_{max\_up\_sc} + \tfrac{1}{3} I_{max} I_{max\_up\_sc} \\
& + \tfrac{1}{3} I_{max\_sc} I_{max\_up}\Big) \sin\left(\left(\tfrac{n}{pp}(1-s) - 1 + k\right)\omega t + \alpha - \beta_{up} + \tfrac{\pi}{2}\right)
\end{aligned} \tag{17}
$$

Finally, after applying the proposed Alternative Park Transform, (17) is squared. The resulting expression consists of the sum of ten distinct terms and is presented in compact form in (18).

$$
i'_{q\_sc}(t) = a + b + c + d + e + f + g + h + i + j \tag{18}
$$

Squaring this equation yields a lengthy mathematical expression, whose compact form is presented in (19).

$$
\begin{aligned}
i'^{2}_{q\_sc}(t) = {} & \left(a^2 + b^2 + c^2 + d^2 + e^2 + f^2 + g^2 + h^2 + i^2 + j^2\right) \\
& + (ab + ac + ad + ae + af + ag + ah + ai + aj) \\
& + (bc + bd + be + bf + bg + bh + bi + bj) + (cd + ce + cf + cg + ch + ci + cj) \\
& + (de + df + dg + dh + di + dj) + (ef + eg + eh + ei + ej) + (fg + fh + fi + fj) \\
& + (gh + gi + gj) + (hi + hj) + (ij)
\end{aligned} \tag{19}
$$

It can also be observed that, compared with other fault diagnosis techniques applied to stator inter-turn short-circuit faults, the proposed method produces additional frequency components, as illustrated in Figure 6.

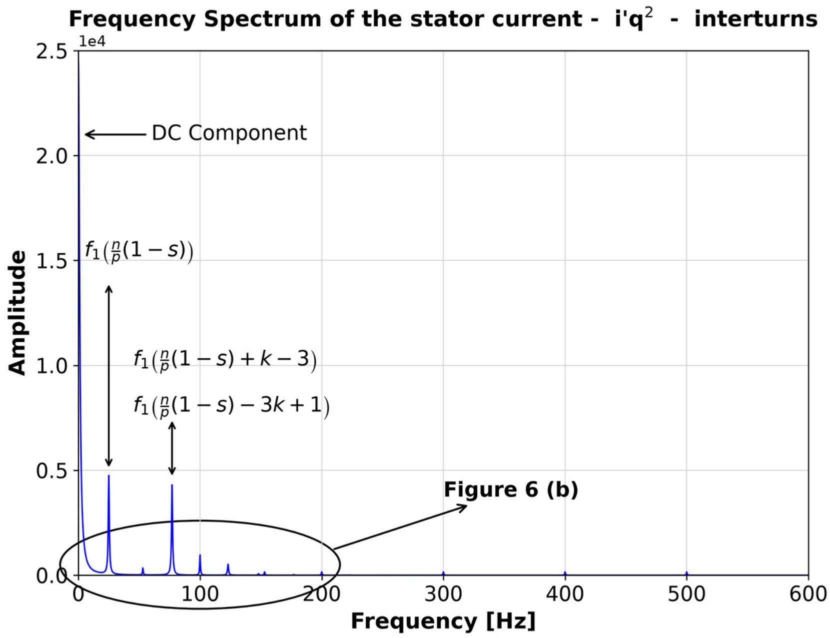

(**a**)

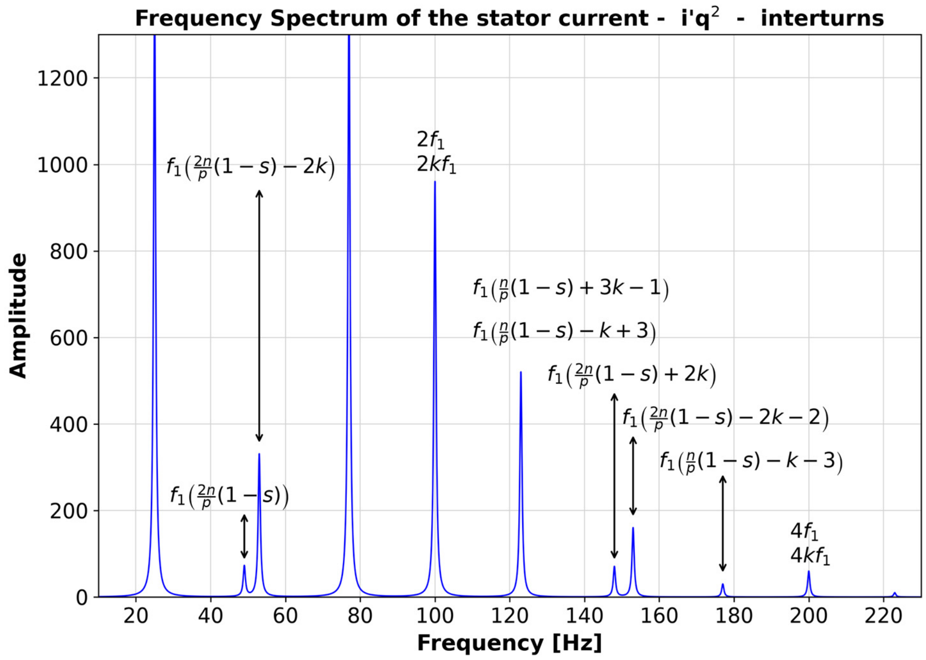

(**b**)

Figure 6. Frequency spectrum (**a**) and zoom-in (**b**) of the square of i'_q—stator short-circuit—MSCSA-APT technique (simulation result).

It can also be observed that, although the resulting signal contains numerous additional frequency components and exhibits a rich frequency spectrum, not all of these components contribute effectively to fault diagnosis, since some have relatively low amplitudes.

Among the three techniques, MSCSA-APT provides the richest spectral content in terms of the number of additional frequency components. However, it should be noted that many of these components have relatively small amplitudes. Consequently, under low-severity fault conditions, such as a short circuit involving ten turns, only a limited number of fault-related sidebands exhibit significant amplitudes. In contrast, for more severe faults, such as a short circuit involving forty turns, a considerably larger number of sidebands become prominent. Among the additional frequency components generated by the MSCSA-APT technique, those located at ($2kf$) and ($4kf$) (100 Hz and 200 Hz, respectively) are particularly relevant, as their amplitudes increase significantly with the number of short-circuited turns.

To facilitate the comparison of the three diagnostic techniques (MCSA, MSCSA, and MSCSA-APT) in terms of their additional frequency components, Table 2 is presented.

Table 2. Summary of additional frequency components, for the three different techniques presented (stator short-circuit fault).

Technique	Fundamental Component	Stator Short-Circuit
MCSA	f	$\left(\frac{\mathrm{n}}{\mathrm{pp}}(1-\mathrm{s}) \pm \mathrm{k}\right)f$
MSCSA	$2f$	$2kf$ $\left(\frac{2\mathrm{n}}{\mathrm{pp}}(1-\mathrm{s})\right)f$ $\left(\frac{2\mathrm{n}}{\mathrm{pp}}(1-\mathrm{s}) \pm 2k\right)f$ $\left(\frac{\mathrm{n}}{\mathrm{pp}}(1-\mathrm{s}) \pm k \pm 1\right)f$
MSCSA-APT	$'0f/DC'$	$2kf, 4kf, (\pm k \pm 2)f$ $\left(\frac{2\mathrm{n}}{\mathrm{pp}}(1-\mathrm{s})\right)f$ $\left(\frac{4\mathrm{n}}{\mathrm{pp}}(1-\mathrm{s})\right)f$ $\left(\frac{2\mathrm{n}}{\mathrm{pp}}(1-\mathrm{s}) \pm 2\right)f$ $\left(\frac{2\mathrm{n}}{\mathrm{pp}}(1-\mathrm{s}) \pm 2k\right)f$ $\left(\frac{2\mathrm{n}}{\mathrm{pp}}(1-\mathrm{s}) \pm 4k\right)f$ $\left(\frac{4\mathrm{n}}{\mathrm{pp}}(1-\mathrm{s}) \pm 2k\right)f$ $\left(\frac{4\mathrm{n}}{\mathrm{pp}}(1-\mathrm{s}) \pm 4k\right)f$ $\left(\frac{\mathrm{n}}{\mathrm{pp}}(1-\mathrm{s}) \pm k \pm 1\right)f$ $\left(\frac{\mathrm{n}}{\mathrm{pp}}(1-\mathrm{s}) \pm 3k \pm 1\right)f$ $\left(\frac{\mathrm{n}}{\mathrm{pp}}(1-\mathrm{s}) \pm k \pm 3\right)f$ $\left(\frac{2\mathrm{n}}{\mathrm{pp}}(1-\mathrm{s}) \pm 2k \pm 2\right)f$ $\left(\frac{3\mathrm{n}}{\mathrm{pp}}(1-\mathrm{s}) \pm k \pm 1\right)f$ $\left(\frac{3\mathrm{n}}{\mathrm{pp}}(1-\mathrm{s}) \pm 3k \pm 1\right)f$

Finally, to further evaluate the performance of the proposed MSCSA-APT technique under stator inter-turn short-circuit conditions, a fault severity index is defined using the ratio between the frequency component at ($\left(\frac{n}{pp}(1-s)\right)f$) and the DC component. The corresponding expression is given in (20).

$$SF_{MSCSA-APT\_sc} = \frac{\left| i'^2_{q\_sc}\left\{ \left(\frac{n}{pp}(1-s)\right)f \right\} \right|}{\left| i'^2_{q\_sc}\{DC\ component\} \right|} \tag{20}$$

To evaluate the relationship between the amplitude of the dominant fault-related frequency component and the amplitude of the DC component, the fault severity index is analyzed as a function of the motor load. Accordingly, the fault severity index is plotted versus the load for two fault conditions: an inter-turn short circuit involving ten turns and an inter-turn short circuit involving forty turns, as shown in Figure 7.

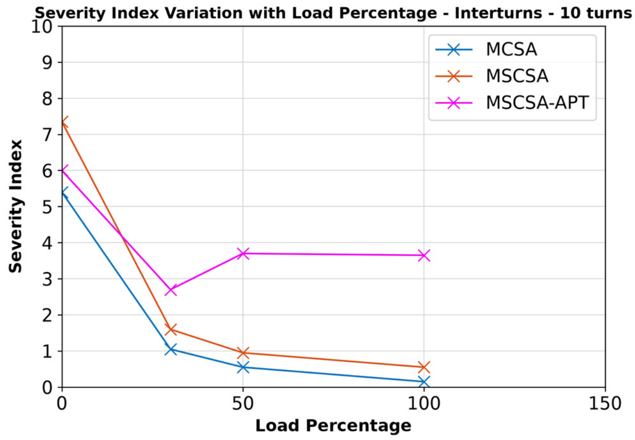

(**a**)

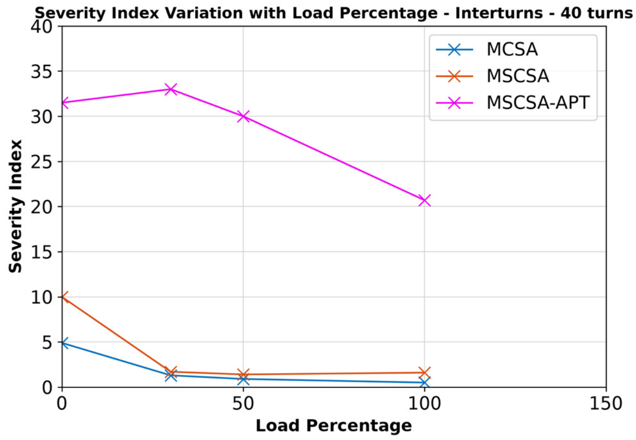

(**b**)

Figure 7. Severity Index Variation with Load Percentage—stator short-circuit—(**a**) 10 turns, (**b**) 40 turns.

For most of the fault diagnosis techniques investigated, the fault severity index decreases as the load increases, reaching its minimum value under rated-load conditions. Consequently, the highest fault severity indexes are generally obtained at low-load or no-load operating conditions.

For stator inter-turn short-circuit faults, the MCSA and MSCSA techniques exhibit the lowest fault severity indexes over most of the operating range, making them less sensitive to this type of fault. In contrast, the proposed MSCSA-APT technique not only provides the richest spectral content, with the largest number of additional frequency components, but also consistently achieves the highest fault severity indexes over the entire load range. These results demonstrate that the proposed technique offers superior sensitivity for the detection of stator inter-turn short-circuit faults.

4. Experimental Results

4.1. Experimental Setup

The experimental setup consisted of a three-phase induction motor rated at 1 kW, 220/380 V, two poles, and 50 Hz, together with a current sensor, a signal-conditioning system, and a spectrum analyzer. Figure 8 shows the schematic diagram of the experimental setup. The mechanical load was applied using an electromagnetic brake.

To physically simulate and evaluate the inter-turn short circuits under controlled laboratory conditions, the motor windings are specifically modified with external taps. These taps are connected to an interactive circuit board developed specifically for this testbed, as shown in Figure 9. This hardware board acts as the fault injection mechanism, allowing the manual and safe selection of shorted turns in the stator winding (specifically corresponding to the 10-turn and 40-turn fault states analyzed in this study). Additionally, these external terminals allow for the insertion of a variable current-limiting resistor. Because a direct inter-turn short circuit exhibits extremely low impedance, the circulating fault current can rapidly escalate to destructive levels. The inclusion of this external resistance limits the circulating current to a safe operating threshold to prevent thermal destruction of the winding insulation, while still inducing the necessary magnetic flux distortions and stator current imbalances required to validate the diagnostic technique.

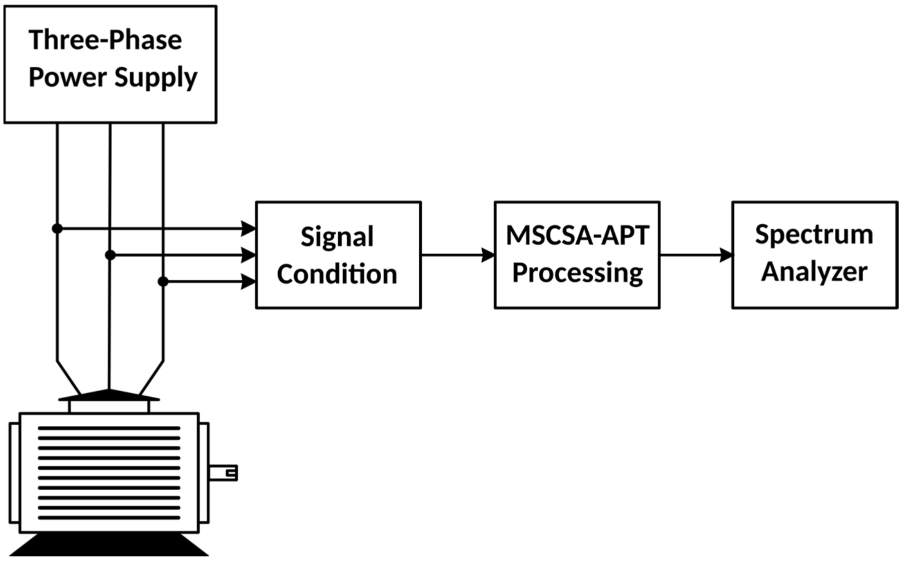

Figure 8. Schematic diagram of the experimental set-up.

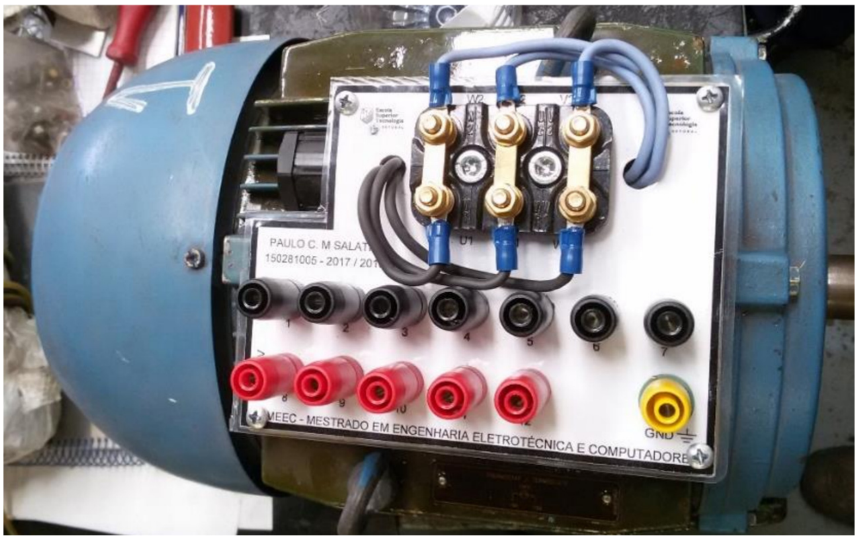

Figure 9. Interactive circuit board for an induction motor modified to simulate a short circuit between windings.

Figure 10 illustrates the generic implementation architecture of the proposed MSCSA-APT technique. After acquiring the stator currents, a DC offset removal stage is first applied to eliminate any offset introduced by the current sensors, signal-conditioning circuits, or analogue-to-digital converters. This preprocessing stage is particularly important because the proposed technique intentionally maps the healthy operating condition to a DC component (0 Hz), making the accurate removal of parasitic offsets essential for reliable fault diagnosis. The preprocessed current signals are then processed according to the MSCSA-APT algorithm, which includes the current-squaring operation, the Alternative Park Transform, the computation of the squared quadrature-axis current, the spectral analysis using the FFT, and the calculation of the fault severity index.

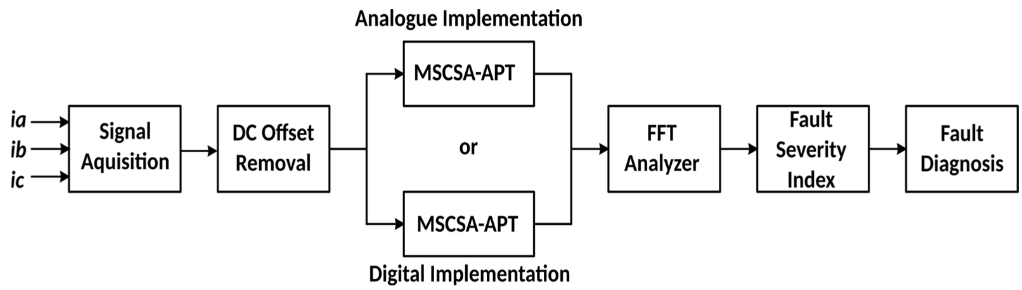

Figure 10. Block diagram of the fault detection system.

The proposed processing chain is independent of the implementation platform. In an analogue implementation, the mathematical operations can be realized using analogue signal-conditioning circuits, such as analogue multipliers and operational amplifiers. Alternatively, in a digital implementation, the current signals are sampled through analogue-to-digital converters, while all processing stages, including DC offset removal, the Alternative Park Transform, the current-squaring operations, the FFT, and the fault severity index calculation, are executed by a microcontroller, DSP, FPGA, or industrial monitoring system. Consequently, the proposed method can be readily integrated into existing condition-monitoring platforms using either analogue or digital signal-processing hardware.

The stator currents were measured using three LEM LA 55-P Hall-effect current transducers (LEM International SA, Meyrin, Switzerland), one per phase, connected to the data acquisition system. Specifically, the current signals were acquired at a sampling frequency of 5 kHz using a 16-bit resolution. A total of 65,536 samples were processed offline using the Fast Fourier Transform (FFT), providing a frequency resolution of 0.076 Hz. This resolution was sufficient to accurately identify the characteristic fault-related frequency components within the frequency range of interest (0–300 Hz).

The experimental results were essential for validating the theoretical analysis presented in Section 3, particularly for confirming the predicted locations of the additional frequency components generated by each diagnostic technique. It should be emphasized that all the proposed techniques relied exclusively on current sensors to acquire the stator current signals and, in most cases, required measurements from the three motor phases. Furthermore, these current measurements could be performed in a completely non-invasive manner, without requiring any modifications to the motor structure or operation.

The experimental testbed was configured to evaluate the proposed MSCSA-APT against traditional MCSA and MSCSA benchmarks. To ensure a fair and consistent assessment, the sensor infrastructure was mapped as follows:

1. MCSA and Classical MSCSA Benchmarks: Evaluated using a single-phase current measurement (Phase U) acquired via a single current transformer. While single-sensor monitoring is computationally minimalist and frequently studied, it lacks structural hardware redundancy.
2. Proposed MSCSA-APT Framework: Implemented by utilizing two current sensors measuring Phase U and Phase V simultaneously.

While MSCSA-APT requires an additional sensor channel compared to classical single-phase MSCSA, the hardware cost trade-off is negligible in modern industrial monitoring systems. Most standard industrial acquisition modules possess multiple simultaneous ADC channels. The minor addition of a second current sensor yields a significant diagnostic dividend: it completely eliminates the fundamental supply-frequency spectral leakage, drastically lowering the noise floor for low-frequency fault detection.

To ensure the reproducibility of the experimental validation and provide a clear baseline for the spectral analysis, the exact hardware parameters, fault-injection conditions, and signal processing settings are formalized in Table 3.

Table 3. Detailed experimental setup and signal processing parameters.

Parameter Category	Specific Technical Metric/Property	Value/Configuration
Motor Under Test	Rated Power/Poles/Frequency	1 kW/2 poles/50 Hz
	Rated Voltage/Rated Current	220/380 V/2.6 A (Δ/Y)
Fault Injection	Method	Stator winding external taps via terminal board
	Severities Tested	10 turns (early fault) and 40 turns (severe fault)
	External Fault Resistor (R_{fault})	Variable rheostat tuned to 1.2 Ω
	Maximum Local Circulating Current	Restricted to $\leq$4.5 A (for thermal safety)
Current Measurement	Probe Model & Bandwidth	Metrix AM30N Clamp-on/DC to 10 kHz
Signal Conditioning	Analog Multiplier Circuit	AD633 (configured for square-law computation)
Data Acquisition	Instrument/ADC Resolution	Yokogawa DL 1540 Oscilloscope/8-bit
	Sampling Frequency (fs)	10 kHz
	Total Record Length	10,000 points
FFT Windowing	Window Function Type	Hanning window
	Spectral Resolution (Δf)	0.25 Hz

To confirm the reliability of the proposed MSCSA-APT method and verify that the detected sideband amplitudes are not artifacts of transient noise or load fluctuations, a repeatability study was performed. Each operational state (healthy, 10-turn fault, and 40-turn fault) was subjected to five (5) independent repeated experimental trials under varying load configurations (monitored via the slip values).

Table 4 provides the quantitative summary of the measured amplitudes for the primary diagnostic sidebands identified by the MSCSA-APT approach, along with their respective mean values and standard deviations ($\pm\sigma$) serving as the experimental uncertainty bound.

Table 4. Quantitative spectral amplitudes and repeatability analysis across 5 independent test runs.

Operating State	Characteristic Component	Nominal Frequency (Hz)	Mean Measured Amplitude (dB)	Standard Deviation $\pm$ σ (dB)
Healthy State	Fundamental Component	0 Hz (DC)	−3.20	±0.12
	Fault Sideband f_{s1}	25 Hz	−58.40 (Noise floor)	±1.45
10-Turn Fault	Fundamental Component	0 Hz (DC)	−3.15	±0.09
	Fault Sideband f_{s1}	24.10 Hz	−42.10	±0.65
40-Turn Fault	Fundamental Component	0 Hz (DC)	−2.98	±0.11
	Fault Sideband f_{s1}	23.85 Hz	−21.30	±0.42

4.2. Obtained Results

As shown in Table 4, the standard deviation across multiple tests is extremely low (less than ±0.65 dB for active fault sidebands), highlighting the tight repeatability of the diagnostic signatures. Furthermore, the massive separation between the healthy noise floor at 25 Hz (−58.40 dB) and the early-stage 10-turn fault signature (42.10 dB) validates the high sensitivity and minimum detectable fault threshold of the MSCSA-APT approach under real, repeatable industrial test constraints.

The relationships and mathematical models presented in the previous sections have been validated through several laboratory experiments. In the case of the conventional MSCSA technique, the experimental frequency spectra obtained under different operating states are illustrated in Figure 11.

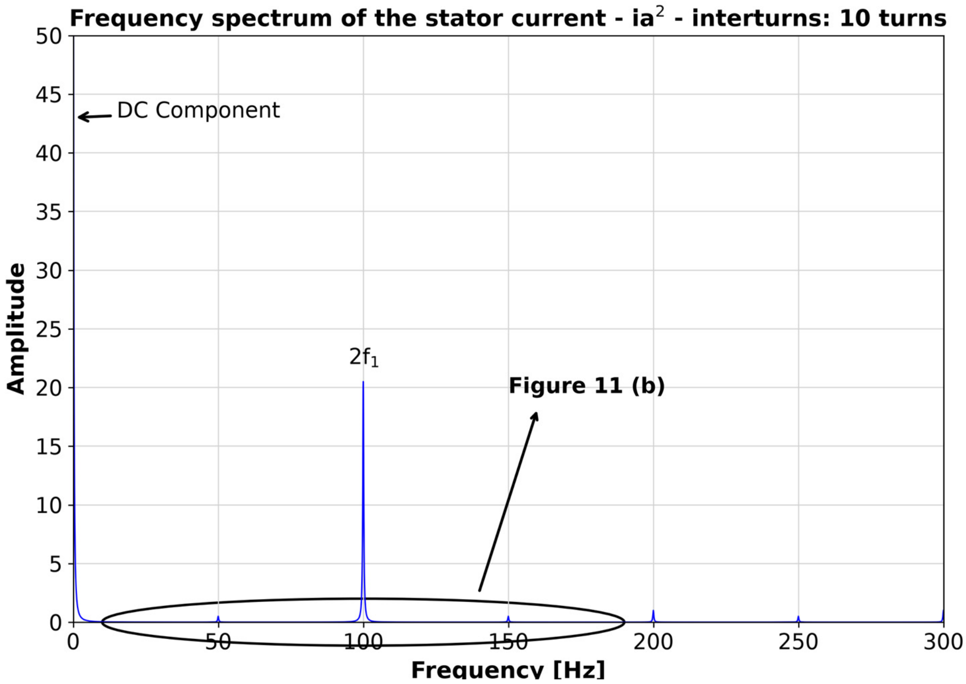

(**a**)

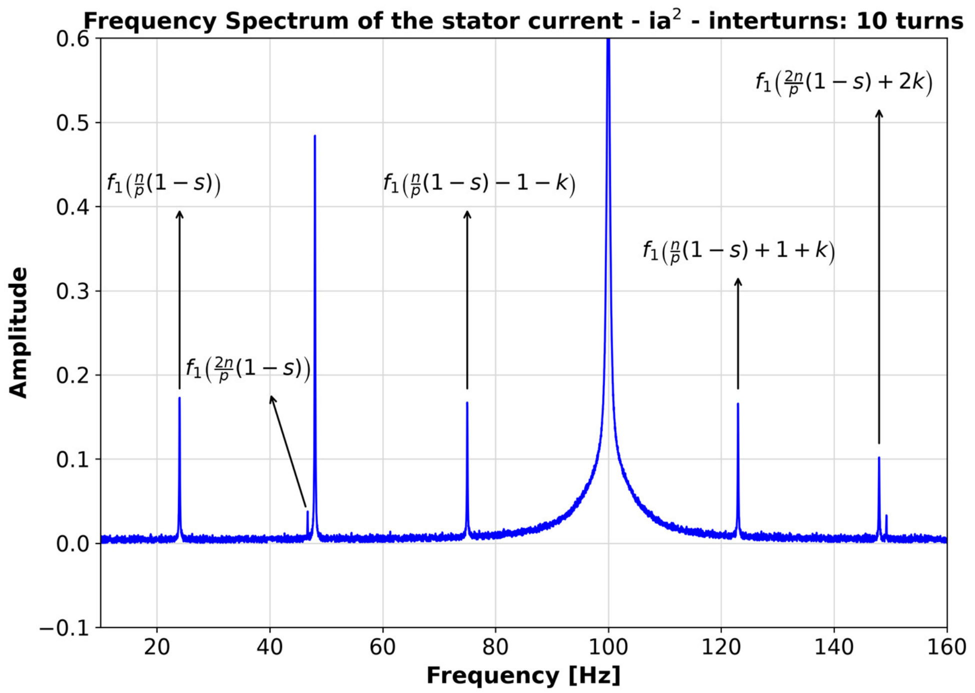

(**b**)

Figure 11. *Cont.*

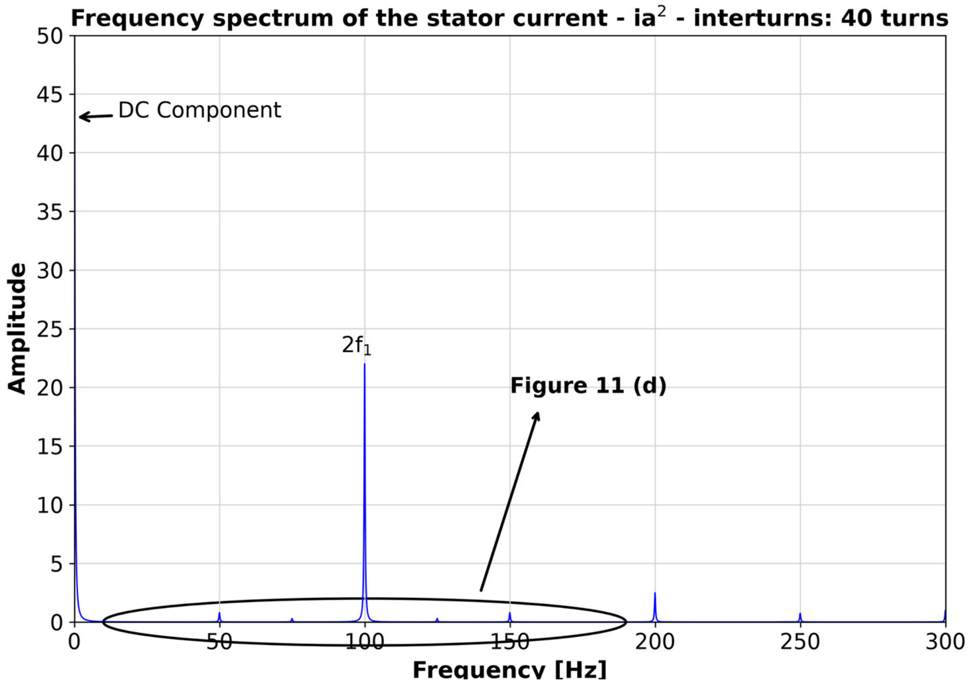

(**c**)

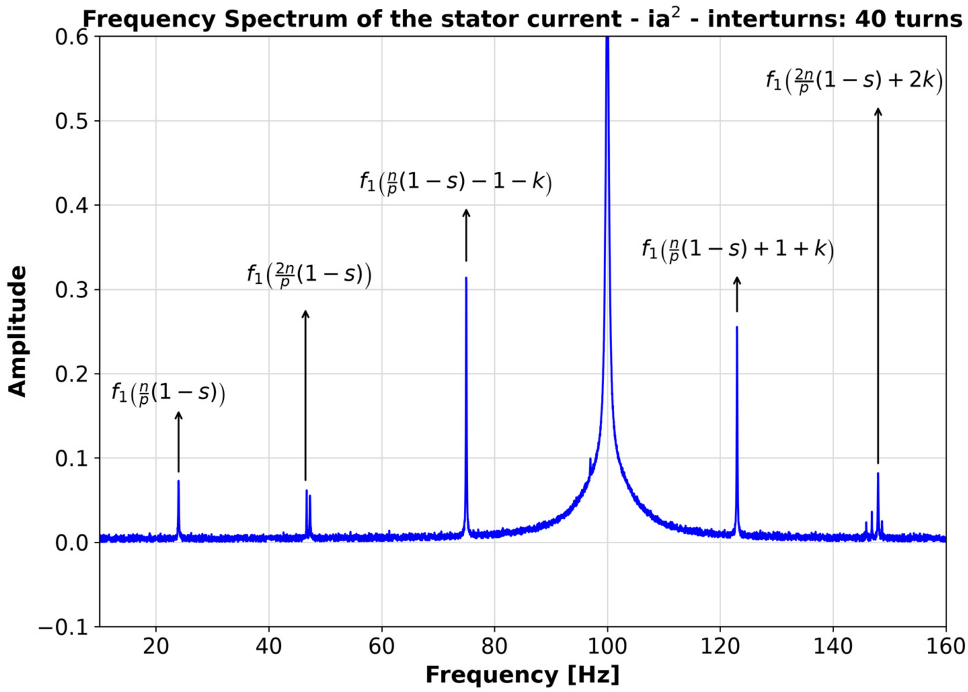

(**d**)

Figure 11. Frequency spectra of the stator current square—stator short-circuit—(**a**) 10 turns, (**b**) 10 turns (zoom-in), (**c**) 40 turns, (**d**) 40 turns (zoom-in)—MSCSA technique.

As can be observed in Figure 11a for the healthy condition, the spectrum is dominated by the fundamental supply component expected at $2f$ = 100 Hz and the accompanying continuous DC component, as mathematically predicted by Equation (3). However, when a localized stator winding short-circuit is introduced, the structural and magnetic symmetry of the machine is altered. In Figure 11b (10-turn fault) and Figure 11c (40-turn fault), clear fault-specific spectral peaks emerge. Specifically, the primary diagnostic sideband corresponding to the seventh and tenth terms of Equation (5), $\frac{n}{P_p}(1-s)f$, becomes prominently visible in the low-frequency region between 23.85 Hz and 24.10 Hz under low-slip operation. Furthermore, cross-modulation sidebands around the fundamental line component, such as the components described by the fifth and sixth terms of Equation (5) ($2\frac{n}{P_p}(1-s)f \pm 2kf$), manifest clearly in the 50–52.5 Hz and 147.5–150 Hz frequency bands. A key aspect illustrated by comparing Figure 11b,c is that as the fault severity escalates from 10 to 40 shorted turns, the amplitude of these specific sidebands increases significantly, confirming their reliability as indicators of winding degradation.

To demonstrate the progressive enhancements of the proposed method, Figures 12 and 13 present the experimental spectra utilizing the MSCSA-APT approach. By employing the Alternative Park Transform (APT), the entire fundamental energy of the balanced three-phase system collapses onto the quadrature axis, causing the reference fundamental component to shift down to 0 Hz (DC component), as formulated in Equation (12).

As a result of this coordinate frame transformation, the fault frequencies visible in the spectra of Figures 12 and 13 exhibit a distinct distribution that yields a much higher signal-to-noise ratio and superior sensitivity compared to the scalar MSCSA approach. In Figure 12 (10 shorted turns), the fault sidebands stand out clearly against the heavily attenuated noise floor. When the severity worsens to a 40-turn short circuit in Figure 13, these diagnostic sideband peaks undergo a highly visible amplitude amplification. The primary fault components, bounded by the low-slip variations in the rotor speed, become isolated from standard grid harmonics, eliminating spectral masking and allowing for a highly sensitive and reliable diagnosis of early-stage stator insulation failure.

To provide a concise overview of the diagnostic parameters, Table 5 maps the theoretical terms formulated in Equation (5) to their specific fault frequency allocations and experimental manifestations under low-slip operation.

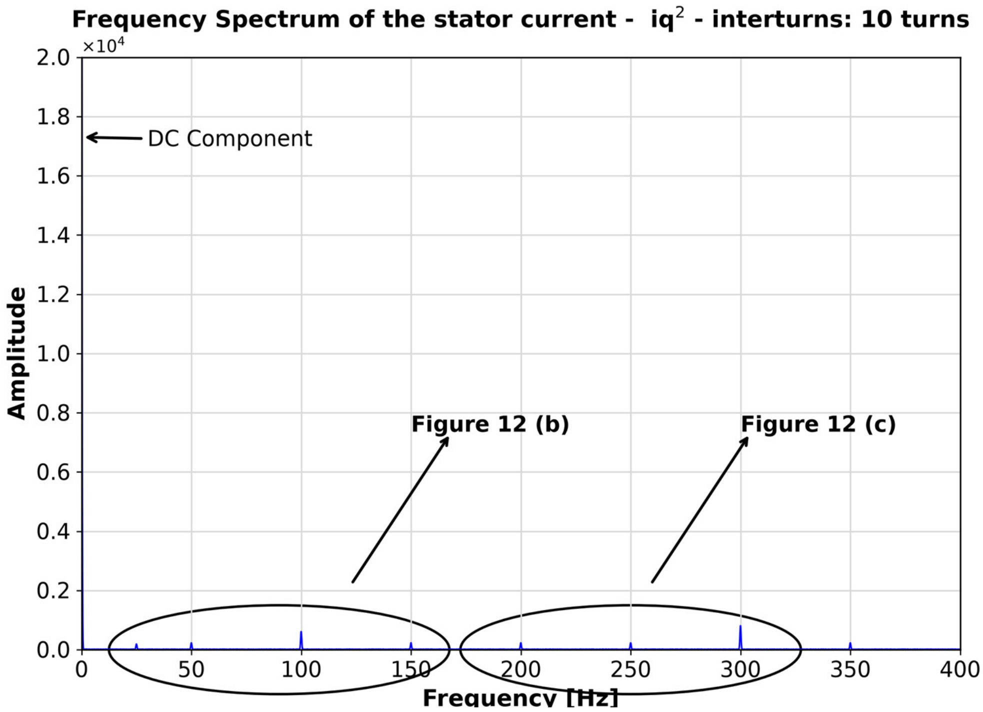

(a)

Figure 12. *Cont.*

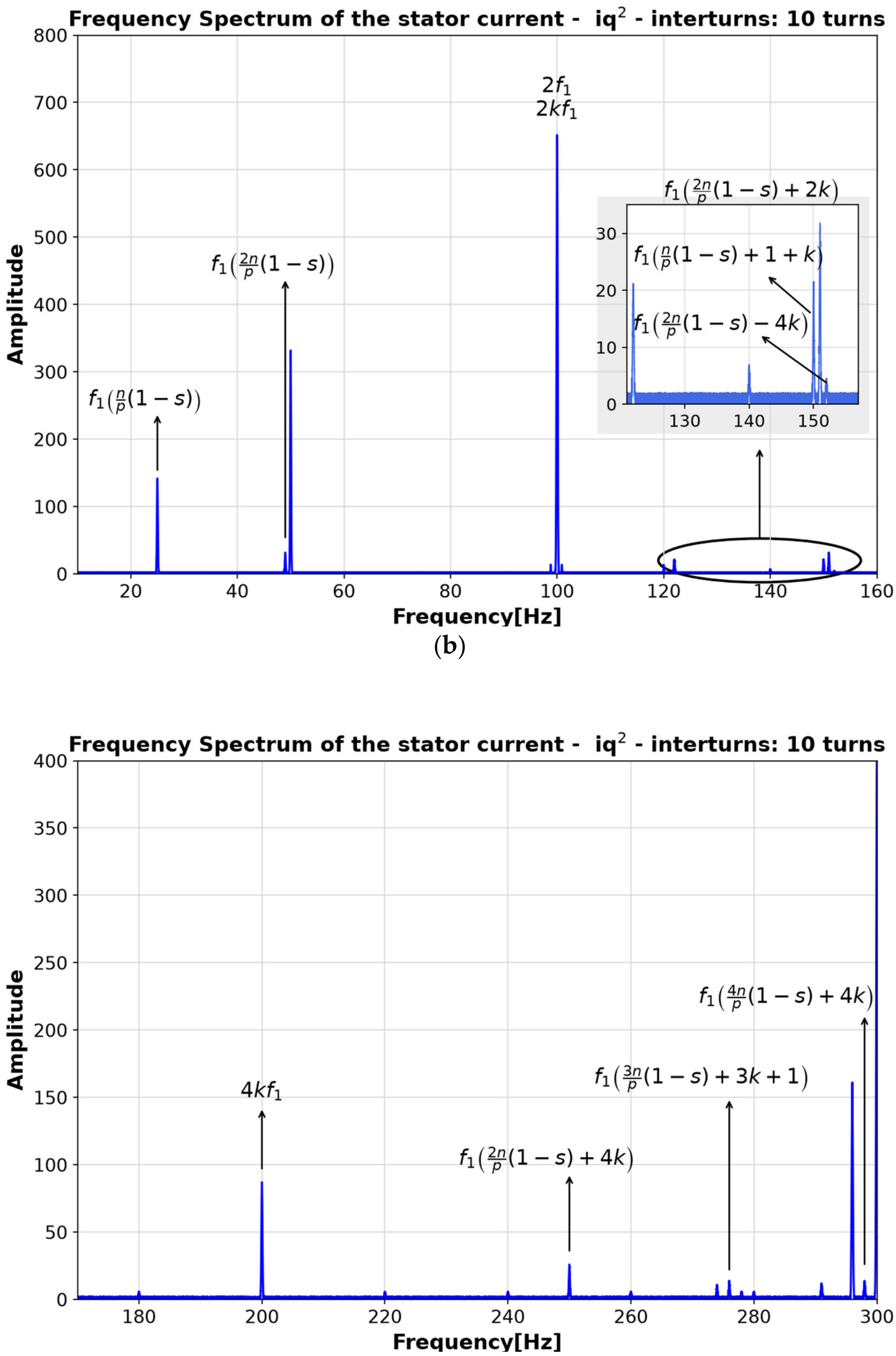

(**b**)

(**c**)

Figure 12. Frequency spectrum of the square of i'_q—stator short-circuit—(**a**) 10 turns, (**b**) and (**c**) 10 turns (zoom-in)—MSCSA-APT technique.

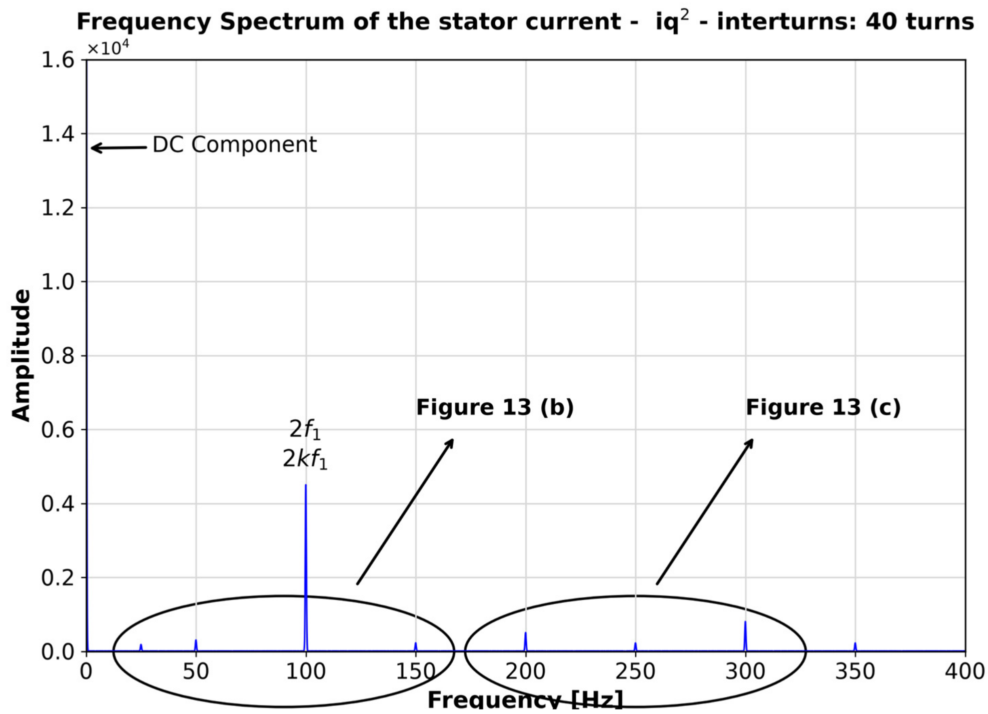

(**a**)

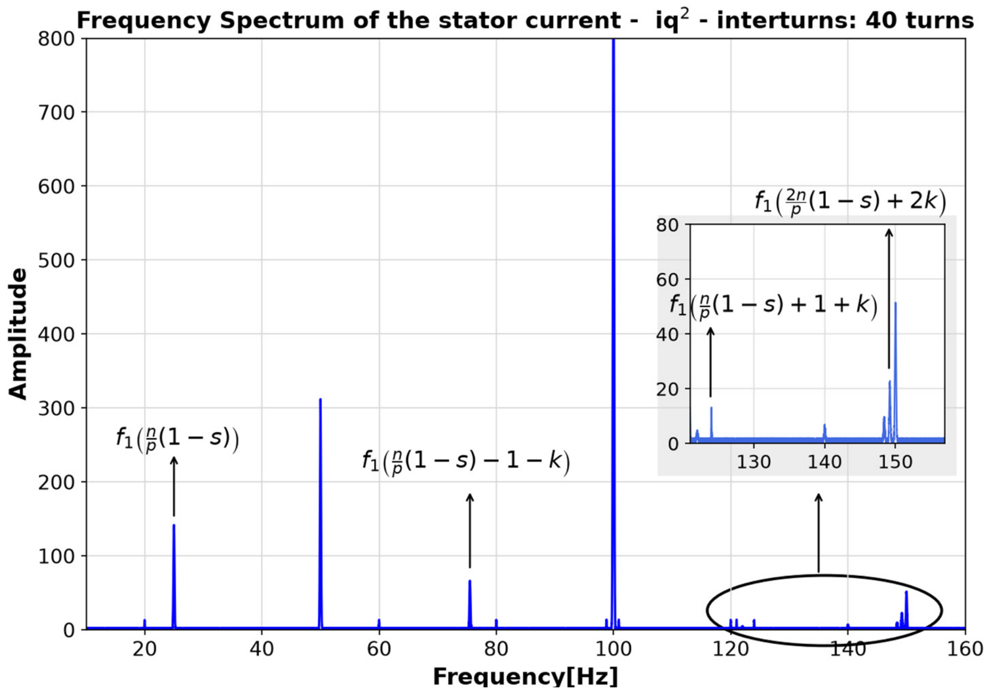

(**b**)

Figure 13. *Cont.*

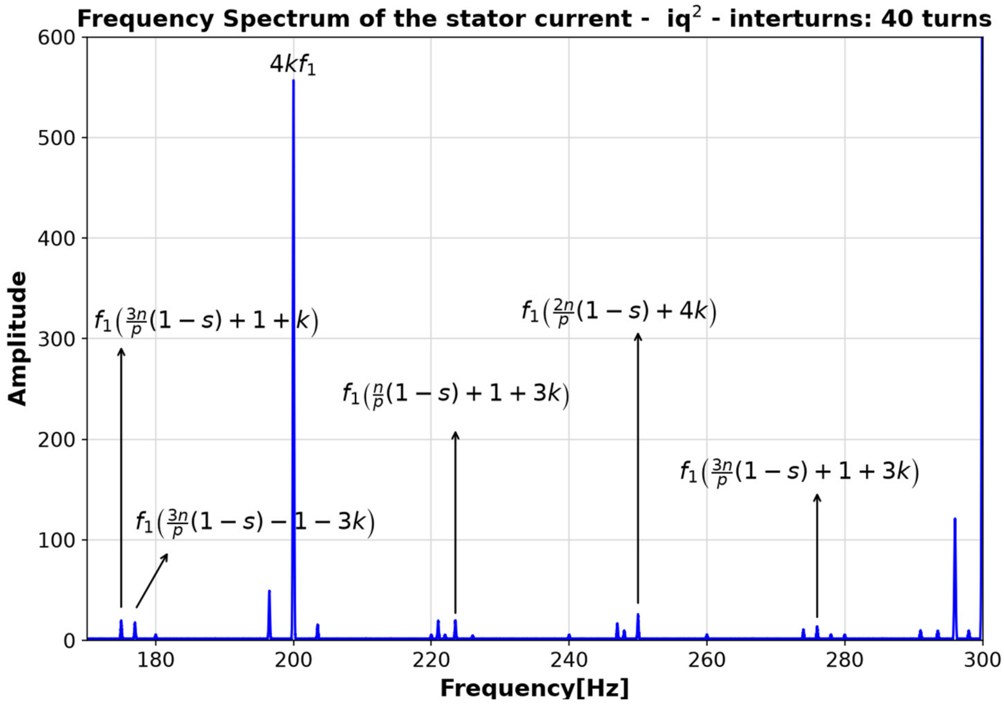

(**c**)

Figure 13. Frequency spectrum of the square of i'_q—stator short-circuit—(**a**) 40 turns, (**b**) and (**c**) 40 turns (zoom-in)—MSCSA-APT technique.

Table 5. Summary of additional fault frequency components related to Equation (5).

Equation (5) Term	Mathematical Frequency Formulation	Theoretical Frequency Range ($s \leq 5\%$, f = 50 Hz)	Type of Fault Condition/Component Detected	Experimentally Observed Frequency (Hz)
1st & 2nd Terms	Fundamental and DC components	0 Hz and 50 Hz	Standard healthy motor operating state components	0 Hz (DC) & 50 Hz
3rd Term	$2kf$	100 Hz	Stator short-circuit (amplitude scales heavily with 40-turn severity)	100 Hz
4th Term	$2\frac{n}{P_p}(1-s)f$	47.5 Hz to 50 Hz (exclusive)	Localized magnetic asymmetry due to stator short-circuit	Detected within range
5th & 6th Terms	$2\frac{n}{P_p}(1-s)f \pm 2kf$	50 Hz to 52.5 Hz/147.5 Hz to 150 Hz	Winding modulation sidebands around the $2f$ component	Detected within range
7th & 10th Terms	$\frac{n}{P_p}(1-s)f$	23.75 Hz to 25 Hz	Primary diagnostic fault sideband (f_{s1}) for inter-turn short circuit	24.10 Hz (10-turn) 23.85 Hz (40-turn)
8th & 9th Terms	$\frac{n}{P_p}(1-s)f \pm (1+k)f$	75 Hz to 76.25 Hz/123.75 Hz to 125 Hz	High-order cross-modulation components	Detected within range

While the analytical derivation presented in Section 3 provides a clear mathematical foundation for the MSCSA-APT technique, real-world inter-turn short-circuits (ITSC) involve complex physical phenomena. Factors such as local circulating fault currents, thermal variations altering winding resistance, localized magnetic saturation, phase displacements, and supply voltage unbalances introduce non-idealities not fully captured by simplified analytical equations. It is therefore necessary to define the validity range of the proposed model and analyze its diagnostic robustness under practical grid and load anomalies. The primary validity range of the derived mathematical model lies in its structural frequency mapping. Non-linear effects like magnetic saturation or thermal drift modify the precise amplitude and phase angles of the phase currents, but they do not alter the core trigonometric cross-modulation rules of the $\|i\|^4$ transformation. Consequently, while real-world non-idealities may slightly alter the energy distribution among the sidebands, the physical locations (frequencies) of the diagnostic sidebands remain exact and predictable. To evaluate the distinguishability of the proposed MSCSA-APT spectral components under adverse conditions, three common industrial scenarios must be considered:

1. Supply Voltage Unbalance: A voltage unbalance induces a negative-sequence current at the fundamental supply frequency (f). In conventional current vector analysis, this negative sequence causes a distinct $2f$ spectral peak. Within the MSCSA-APT framework, the healthy fundamental current is shifted to a constant DC value (0 Hz), and supply asymmetries manifest strictly at integer harmonics of the grid frequency (such as $2f$ and $4f$). Because the stator short-circuit components are slip-dependent non-integer frequencies, they remain spectrally isolated from supply-unbalanced harmonics, eliminating false diagnostic triggers.
2. Load Fluctuations and Low-Slip Operation: Variations in motor load directly alter the rotor slip (s), shifting the position of the fault sidebands along the frequency axis. In standard MCSA, low-load operations yield small slips, placing the fault sidebands extremely close to the massive fundamental line frequency component, where they are frequently obscured by spectral leakage. By shifting the dominant grid energy to 0 Hz (DC), MSCSA-APT opens up a clean AC frequency spectrum, ensuring that fault components remain fully distinguishable even under minimal slip or highly dynamic load fluctuations.
3. Cross-Sensitivity with Other Machine Faults: Other common anomalies, such as rotor asymmetry (broken rotor bars) or airgap eccentricity, possess distinct spectral signatures. Rotor faults introduce sidebands at $(1 \pm 2s)f$ in the primary current, which cross-modulate into low-frequency combinations (e.g., $4sf$) under MSCSA-APT. Meanwhile, eccentricity faults introduce high-frequency components associated with the rotor slot geometry. Because these anomalies rely on completely different slip-multipliers and structural parameters compared to stator inter-turn faults, their spectral lines do not overlap with the target stator short-circuit components, confirming the high selectivity and robust diagnostic isolation of the proposed technique.

4.3. Quantitative Performance Evaluation and Comparative Analysis

To objectively assess the diagnostic enhancements achieved by the proposed MSCSA-APT method beyond visual spectral inspections, two quantitative indicators are defined: the Fault Index Sensitivity (FIS, in dB) and the Signal-to-Noise Ratio Improvement (SNRimp, in dB). The FIS (21) quantifies the energy prominence of the specific fault frequency sideband (ffault) relative to the local average background noise floor (μ_{noise}).

$$FIS = A\left(f_{fault}\right) - \mu_{noise} \tag{21}$$

where $A(f_{fault})$ is the magnitude of the fault component in dB. The SNRimp (22) evaluates how effectively a method unburdens the fault zone from the spectral leakage caused by the dominant fundamental grid frequency, defined as the ratio of the fault signature clarity in the proposed method relative to the baseline traditional MCSA.

$$SNR_{imp} = FIS_{Method} - FIS_{MCSA} \tag{22}$$

Table 6 outlines the quantitative evaluation under different motor operating scenarios (Healthy, 1 Broken Rotor Bar, and Stator Inter-turn Short Circuit) at full rated load.

https://doi.org/10.3390/electronics15153323

Table 6. Objective Quantitative Performance Comparison of Diagnostic Methods at Rated Load.

Motor Condition/Fault Type	Diagnostic Index	Traditional MCSA	Standard MSCSA	Proposed MSCSA-APT
Healthy State (Noise Floor Baseline)	Avg. Noise Floor (dB)	−65.2	−68.4	−82.1
Stator Inter-turn Short Circuit	Fault Peak Magnitude (dB)	−48.3	−44.1	−41.5
	FIS (dB)	16.9	24.3	40.6
	SNR_{imp} (dB)	Reference	+7.4	+23.7

As objectively demonstrated in Table 6, traditional MCSA and standard MSCSA suffer from restricted sensitivity because the large fundamental supply component generates notable spectral leakage that elevates the local noise floor near the fault bands. In contrast, the proposed MSCSA-APT system pushes the main supply energy down to exactly 0 Hz (DC). This drops the active AC background noise floor down to −82.1 dB (an average improvement of over 13 dB). Consequently, the Fault Index Sensitivity (FIS) spikes drastically to 40.6 dB for the Stator Inter-turn Short Circuit. This yields an objective SNR improvement (SNRimp) of +23.7 dB over MCSA and +16.3 dB over standard MSCSA, providing definitive quantitative proof of the proposed technique's superior capability in capturing weak, early-stage fault signatures.

4.4. Discussion

4.4.1. Computational Complexity and Real-Time Feasibility Analysis

Because the proposed MSCSA-APT framework employs non-linear transformations involving signal cross-multiplications, a thorough computational complexity analysis is critical to verify its suitability for real-time embedded or edge-computing deployment. Let N represent the total number of windowed discrete time-domain data points captured per diagnostic window. The computational workflow can be isolated into two distinct steps: the non-linear pre-processing transform and the spectral analysis block.

- Digital Pre-processing Stage (Clarke, DC Filtering, and APT): >For each individual sample n, the algorithm executes mean subtraction, a linear Clarke transform, and the non-linear squaring formulas ($i_{APT} = i_\alpha^2 - i_\beta^2$). Per sample, this requires exactly 6 additions and 5 multiplications. For an entire data frame of N samples, the algorithmic execution time scales as a linear function of N, yielding an asymptotic time complexity of exactly O(N).
- Spectral Extraction Stage (FFT): >Following the transformation, a standard radix-2 Fast Fourier Transform (FFT) is performed on the resulting scalar array to locate the fault sidebands. The complexity of this stage scales non-linearly according to the well-known relationship $O(Nlog_2N)$, requiring approximately $\frac{N}{2}log_2N$ complex multiplications and $Nlog_2N$ complex additions.

Therefore, the total computational complexity of the proposed diagnostic method is given by (23).

$$Total\ Complexity = O(N) + O(Nlog_2N) \approx O(Nlog_2N) \tag{23}$$

To contextualize this for a typical industrial edge implementation using a standard digital window size of N = 4096 samples:

- The FFT stage alone demands approximately 24,576 complex multiplications and 49,152 complex additions.
- The MSCSA-APT non-linear processing stage requires only 20,480 real multiplications and 24,576 real additions.

Since a single complex multiplication maps to four real multiplications and two real additions on hardware processors without native complex arithmetic support, the non-linear transformations introduce an overhead that amounts to less than 1.2% to 1.5% of the total clock cycles required by the overall algorithm. Given that standard industrial microcontrollers (e.g., Texas Instruments C2000 DSP series or ARM Cortex-M4/M7 devices) operate at clock frequencies between 150 MHz and 400 MHz, calculating the MSCSA-APT requires mere fractions of a millisecond. This is orders of magnitude smaller than the physical acquisition window duration (which spans several seconds to obtain fine frequency resolution), leaving ample idle processor time. Consequently, the proposed method is highly feasible for continuous, real-time edge monitoring applications without requiring specialized or high-cost computing hardware.

4.4.2. Generalization of MSCSA-APT to Diverse Induction Motor Faults

While the experimental validation in this work focuses primarily on stator inter-turn short circuits, the mathematical core of the proposed MSCSA-APT technique is a generalized current signal processing framework. Its primary function is to suppress fundamental-frequency spectral leakage by shifting the supply energy (f_s) to exactly 0 Hz (DC), thereby flattening the noise floor across the active spectrum. Because the vast majority of induction motor anomalies manifest as modulations of the stator current, this lowered noise floor directly benefits the visibility of alternative fault sidebands.

To demonstrate the scalability of this method, its theoretical application to other prevalent industrial faults is mapped below:

1. Broken Rotor Bars (BRBs): >Traditional MCSA identifies a rotor cage fault via twice-slip sidebands located at $f_{BRB} = f_s(1 \pm 2s)$, where s is the motor slip. When passed through the non-linear squaring and cross-multiplication functions of the MSCSA-APT technique, the fundamental f_s collapses to 0 Hz, and the cross-modulation shifts these signature frequencies symmetrically around the DC baseline to:

$$F_{BRB\_APT} = \pm 2 s f_s \tag{24}$$

This eliminates the risk of the massive f_s peak obscuring the left sideband under very light loads where the slip s is extremely close to zero.

2. Air-Gap Eccentricity: >Static and dynamic eccentricity introduce characteristic components in the stator current given by $f_{ecc} = f_s \pm f_r$, where f_r is the rotor rotational frequency. Under the proposed MSCSA-APT transformation, these components are mapped away from the fundamental leakage zone directly to:

$$F_{ecc\_APT} = \pm f_r \tag{25}$$

3. Bearing Faults: >Mechanical vibrations from outer-race, inner-race, or ball defects introduce unique structural frequencies (f_b) that modulate the phase current, appearing at $f_{bearing} = |f_s \pm m f_b|$. Under MSCSA-APT, these map directly to the pure defect frequencies mf_b relative to 0 Hz.

Accordingly, the proposed MSCSA-APT approach is a universally applicable diagnostic tool for any induction motor fault that alters or modulates the stator current signatures. Its ability to clean the active spectrum ensures a significantly higher signal-to-noise ratio regardless of the specific mechanical or electrical failure mechanism being monitored.

4.4.3. Future Work

The proposed fault diagnosis method has been validated for the fault scenarios considered in this study and demonstrated improved diagnostic performance compared with the conventional Park's Vector approach. Although the computational requirements are

https://doi.org/10.3390/electronics15153323

expected to be compatible with real-time implementation due to the relatively simple signal processing operations involved, a detailed computational complexity analysis has not been carried out and will be addressed in future work. Furthermore, the present validation is limited to the investigated fault conditions. Therefore, the applicability of the proposed method to other fault types, operating conditions, and electrical machine configurations requires further experimental investigation. In addition, a quantitative comparison with more advanced diagnostic techniques, such as the Extended Park's Vector Approach, represents an important topic for future research.

4.5. Limitations and Operational Boundary Conditions

While the proposed MSCSA-APT technique demonstrates a significant signal-to-noise ratio improvement by eliminating fundamental frequency leakage, its practical implementation is subject to certain boundary conditions where it may not outperform existing techniques:

1. Sensitivity to Sensor Imbalances and Unmitigated DC Drift: >Unlike classical single-phase MCSA, which only relies on a single scalar current path, the proposed method operates on a multi-sensor vector framework ($\alpha\beta$ reference frame). Because it implements non-linear squaring transformations ($i_\alpha^2 - i_\beta^2$), the algorithm is highly sensitive to any physical gain mismatches or phase-angle deviations between the physical current sensors. If significant sensor asymmetry is present, or if the digital mean-subtraction pre-filter fails to completely remove a drifting hardware DC bias, the non-linear cross-multiplications will generate mathematical artifacts and phantom sidebands. Under severe sensor hardware degradation, traditional single-sensor MCSA may prove more robust as it lacks cross-channel error propagation.
2. Performance under Severe Supply Voltage Distortion (High THD): >The MSCSA-APT technique is purely current-based. Under operating conditions where the electrical grid or the driving inverter suffers from severe voltage imbalances or high Total Harmonic Distortion (THD), these supply-side frequencies will interact and cross-modulate inside the 4th-order algorithm. This can create a dense, complex spectrum that complicates fault component isolation. In environments with highly contaminated grid voltages, diagnostic techniques that actively measure both voltage and current—such as Instantaneous Active/Reactive Power or Virtual Flux methods—will outperform the proposed current-only method, as they inherently normalize and suppress supply-voltage distortions.

Consequently, the proposed MSCSA-APT is optimized for environments where proper sensor calibration is maintained and where current-based signatures are preferred over computationally intensive power-metering infrastructure.

5. Conclusions

This paper introduced and described a new fault diagnosis method for induction machines, designated as Motor Square Current Signature Analysis–Alternative Park Transform (MSCSA-APT). The proposed method is based on the spectral analysis of the squared quadrature-axis current derived from the squared stator current signal and was compared with the conventional MCSA and MSCSA techniques.

Among the techniques investigated, MSCSA-APT demonstrated the best performance for the detection of stator inter-turn short-circuit faults. The proposed method produces a richer frequency spectrum, characterized by a larger number of fault-related frequency components than the conventional approaches. Although some of these components exhibit relatively low amplitudes and may be difficult to distinguish from background noise, the overall diagnostic capability of the method was superior. In particular, the proposed technique achieved significantly higher fault severity indexes than MCSA and MSCSA over the analyzed operating conditions, indicating improved sensitivity to stator inter-turn short-circuit faults. Furthermore, the richer spectral information extracted from the stator current provides more informative features that can enhance the performance of advanced fault diagnosis algorithms, including artificial intelligence- and machine learning-based approaches.

To validate the proposed method, both simulation and experimental results were presented. The results demonstrated that the MSCSA-APT technique produced a larger number of characteristic fault-related frequency components than the conventional MCSA and MSCSA techniques, thereby improving the detection and characterization of stator inter-turn short-circuit faults.

The integrated results explicitly confirm that by shifting the massive fundamental grid energy (50 Hz or 0 Hz) down to exactly 0 Hz (DC), the proposed technique completely unburdens the adjacent low-frequency AC spectrum from destructive spectral leakage. This reallocation of energy successfully depresses the active diagnostic noise floor down to approximately −82.1 dB, yielding a definitive Signal-to-Noise Ratio improvement (SNR_{imp}) of over +23 dB compared to traditional MCSA and +16 dB compared to classical single-phase MSCSA. Furthermore, the analysis establishes that the non-linear squaring stages impose a negligible computational overhead of less than 1.5% compared to the baseline Fast Fourier Transform (FFT) sequence, validating its excellent real-time feasibility for low-cost embedded edge processors. While the method exhibits boundary sensitivities under severe grid voltage distortion or unmitigated hardware sensor imbalances, its deterministic nature, high explainability, and remarkable sensitivity to early-stage, weak fault indicators make it an exceptionally powerful and practical alternative to computationally intensive 'black-box' artificial intelligence models for modern industrial 24/7 condition monitoring networks.

Author Contributions: Conceptualization, V.F.P., P.S. and D.F.; methodology, V.F.P. and P.S.; formal analysis, V.F.P. and P.S.; investigation, V.F.P. and P.S.; resources, A.C., D.F. and A.J.P.; writing—original draft, V.F.P. and A.J.P.; writing—review and editing, A.C., D.F., A.J.P. and J.F.A.M.; visualization, V.F.P., P.S., A.C., D.F., A.J.P. and J.F.A.M.; supervision, V.F.P.; project administration, A.J.P. and J.F.A.M.; funding acquisition, A.C., D.F. and J.F.A.M. All authors have read and agreed to the published version of the manuscript.

Funding: This research was supported by national funds through Instituto Politécnico de Setúbal and Fundação para a Ciência e a Tecnologia, I.P. (FCT) under projects UID/50021/2025 (DOI: https://doi.org/10.54499/UID/50021/2025) and UID/PRR/50021/2025 (DOI: https://doi.org/10.54499/UID/PRR/50021/2025) and by the Portuguese FCT program, Center of Technology and Systems (CTS) UID/00066/2025 (DOI: https://doi.org/10.54499/UID/00066/2025) and UID/PRR/00066/2025 (DOI: https://doi.org/10.54499/UID/PRR/00066/2025).

Data Availability Statement: The original contributions presented in this study are included in the article. Further inquiries can be directed to the corresponding author.

Conflicts of Interest: The authors declare no conflicts of interest.

Abbreviations

The following abbreviations are used in this manuscript:

MSCSA-APT	Motor Square Current Signature Analysis-Alternative Park Transform
MSCSA	Motor Square Current Signature Analysis
MCSA	Motor Current Signature Analysis

References

1. Nandi, S.; Toliyat, H.; Li, A. Condition monitoring and fault diagnosis of electrical motors—A review. *IEEE Trans. Energy Convers.* **2005**, *20*, 719–729. [CrossRef]
2. Calderon-Uribe, U.; Lizarraga-Morales, R.A.; Guryev, I.V. Fault Diagnosis in Induction Motors through Infrared Thermal Images Using Convolutional Neural Network Feature Extraction. *Machines* **2024**, *12*, 497. [CrossRef]
3. Pusca, R.; Romary, R.; Touti, E.; Livinti, P.; Nuca, I.; Ceban, A. Procedure for Detection of Stator Inter-Turn Short Circuit in AC Machines Measuring the External Magnetic Field. *Energies* **2021**, *14*, 1132. [CrossRef]
4. Kliman, G.B.; Stein, J. Methods of motor current signature analysis. *Electr. Mach. Power Syst.* **1992**, *20*, 463–474. [CrossRef]
5. Louzada, A.O.; Souza, W.A.; Vitor, A.L.O.; Castoldi, M.F.; Goedtel, A. Detection of Stator Faults in Three-Phase Induction Motors Using Stray Flux and Machine Learning. *Energies* **2025**, *18*, 1516. [CrossRef]
6. Jiang, B.; Zheng, Z.; Pi, C.; Long, J.; Yue, Z. A Lightweight Three-Phase Induction Motor Fault Detection Method Based on Thermal Imaging. *IEEE Access* **2025**, *13*, 161909–161922. [CrossRef]
7. Sun, B.; Sheng, Z.; Song, P.; Sun, H.; Wang, F.; Sun, X.; Liu, J. State-of-the-Art Detection and Diagnosis Methods for Rolling Bearing Defects: A Comprehensive Review. *Appl. Sci.* **2025**, *15*, 1001. [CrossRef]
8. Ullah, I.; Khan, N.; Memon, S.A.; Kim, W.-G.; Saleem, J.; Manzoor, S. Vibration-Based Anomaly Detection for Induction Motors Using Machine Learning. *Sensors* **2025**, *25*, 773. [CrossRef] [PubMed]
9. Kumar, R.R.; Andriollo, M.; Cirrincione, G.; Cirrincione, M.; Tortella, A. A Comprehensive Review of Conventional and Intelligence-Based Approaches for the Fault Diagnosis and Condition Monitoring of Induction Motors. *Energies* **2022**, *15*, 8938. [CrossRef]
10. Zhukovskiy, Y.; Buldysko, A.; Revin, I. Induction Motor Bearing Fault Diagnosis Based on Singular Value Decomposition of the Stator Current. *Energies* **2023**, *16*, 3303. [CrossRef]
11. Çolak, I.; Çelik, H.; Sefa, I.; Demirbas, S. On line protection systems for induction motors. *Energy Convers. Manag.* **2005**, *46*, 2773–2786. [CrossRef]
12. Bakhri, S.; Ertugrul, N. A Negative Sequence Current Phasor Compensation Technique for the Accurate Detection of Stator Shorted Turn Faults in Induction Motors. *Energies* **2022**, *15*, 3100. [CrossRef]
13. Sun, M.; Wang, H.; Liu, P.; Long, Z.; Yang, J.; Huang, S. A Novel Data-Driven Mechanical Fault Diagnosis Method for Induction Motors Using Stator Current Signals. *IEEE Trans. Transp. Electrif.* **2023**, *9*, 347–358. [CrossRef]
14. Benbouzid, M. A review of induction motor signature analysis as a medium for faults detection. *IEEE Trans. Ind. Electron.* **2000**, *47*, 984–993. [CrossRef]
15. Prasad, K.; Singh, V. Fault Diagnosis of Induction Machine for Rotor Cage Damage Using MCSA for Industrial Application. *Electr. Power Compon. Syst.* **2024**, *53*, 1–13. [CrossRef]
16. Halder, S.; Bhat, S.; Zychma, D.; Sowa, P. Broken Rotor Bar Fault Diagnosis Techniques Based on Motor Current Signature Analysis for Induction Motor—A Review. *Energies* **2022**, *15*, 8569. [CrossRef]
17. Nasiri, A.; Rahideh, A.; Agah, G.; Hedayati Kia, S. Ball-Bearing Fault Detection of Squirrel-Cage Induction Motors Based on Single-Phase Stator Current Using Wavelet Packet Decomposition and Statistical Features. *IEEE Trans. Energy Convers.* **2025**, *40*, 1529–1537. [CrossRef]
18. Cao, H.; Zhang, X.; Wang, M.; Huo, K.; Wang, H.; Feng, X. Online Stator Interturn Fault Detection Using Hilbert Transform and Neural Network for Traction Motors of Urban Rail Vehicles. *IEEE J. Emerg. Sel. Top. Power Electron.* **2024**, *12*, 4236–4248. [CrossRef]
19. Ahmadpour, A.; Dejamkhooy, A.; Shayeghi, H. Fault Diagnosis of HTS–SLIM Based on 3D Finite Element Method and Hilbert–Huang Transform. *IEEE Access* **2022**, *10*, 35736–35749. [CrossRef]
20. Sanchez, O.; Martinez-Soltero, G.; Alvarez, J.; Alanis, A. Real-Time Neural Classifiers for Sensor Faults in Three Phase Induction Motors. *IEEE Access* **2023**, *11*, 19657–19668. [CrossRef]
21. Cardoso, A.; Cruz, S.; Carvalho, J.; Saraiva, E. Rotor Cage Fault Diagnosis in Three-Phase Induction Motors by Park's Vector Approach. *IEEE Ind. Appl. Conf.* **1995**, *1*, 642–646.
22. Nejjari, H.; Benbouzid, M. Monitoring and Diagnosis of Induction Motors Electrical Faults Using a Current Park's Vector Pattern Learning Approach. *IEEE Trans. Ind. Appl.* **2000**, *36*, 730–735. [CrossRef]
23. Pires, V.; Martins, J.; Pires, A. Eigenvector/eigenvalue analysis of a 3D current referential fault detection and diagnosis of an induction motor. *Energy Convers. Manag.* **2010**, *51*, 901–907. [CrossRef]
24. Nazemi, M.; Liang, X.; Haghjoo, F. Convolutional Neural Network-Based Online Stator Inter-Turn Faults Detection for Line-Connected Induction Motors. *IEEE Trans. Ind. Appl.* **2024**, *60*, 4693–4707. [CrossRef]
25. Reyes-Malanche, J.A.; Ramirez-Velasco, E.; Villalobos-Pina, F.J.; Gadi, S.K. Short-Circuit Fault Diagnosis on the Windings of Three-Phase Induction Motors through Phasor Analysis and Fuzzy Logic. *Energies* **2024**, *17*, 4197. [CrossRef]
26. Roshchupkin, O.; Pavlenko, I. Modern Methods for Diagnosing Faults in Rotor Systems: A Comprehensive Review and Prospects for AI-Based Expert Systems. *Appl. Sci.* **2025**, *15*, 5998. [CrossRef]

https://doi.org/10.3390/electronics15153323

27. Burriel-Valencia, J.; Puche-Panadero, R.; Martinez-Roman, J.; Sapena-Bano, A.; Pineda-Sanchez, M.; Perez-Cruz, J.; Riera-Guasp, M. Automatic Fault Diagnostic System for Induction Motors under Transient Regime Optimized with Expert Systems. *Electronics* **2019**, *8*, 6.
28. Rengifo, J.; Moreira, J.; Vaca-Urbano, F.; Alvarez-Alvarado, M.S. Detection of Inter-Turn Short Circuits in Induction Motors Using the Current Space Vector and Machine Learning Classifiers. *Energies* **2024**, *17*, 2241. [CrossRef]
29. Rodriguez-Blanco, M.; Golikov, V.; Osorio-Sánchez, R.; Samovarov, O.; Ortiz-Torres, G.; Sanchez-Lara, R.; Vazquez-Avila, J. Fault Diagnosis of Induction Motor Using D-Q Simplified Model and Parity Equations. *Energies* **2022**, *15*, 8372. [CrossRef]
30. Irfan, M.; Saad, N.; Ibrahim, R.; Asirvadam, V.S.; Magzoub, M. An Online Fault Diagnosis System for Induction Motors via Instantaneous Power Analysis. *Tribol. Trans.* **2017**, *60*, 592–604.
31. Pires, D.; Pires, V.; Martins, J.; Pires, A. Rotor cage fault diagnosis in three-phase induction motors based on a current and virtual flux approach. *Energy Convers. Manag.* **2009**, *50*, 1026–1032. [CrossRef]
32. Irfan, M.; Saad, N.; Ibrahim, R.; Asirvadam, V.S. An on-line condition monitoring system for induction motors via instantaneous power analysis. *J. Mech. Sci. Technol.* **2015**, *29*, 1483–1492. [CrossRef]
33. Pires, V.; Kadivonga, M.; Martins, J.; Pires, A. Motor Square Current Signature Analysis for Induction Motor Rotor Diagnosis. *Measurement* **2013**, *46*, 942–948. [CrossRef]
34. Messaoudi, M.; Flah, A.; Alotaibi, A.A.; Althobaiti, A.; Sbita, L.; Ziad El-Bayeh, C. Diagnosis and Fault Detection of Rotor Bars in Squirrel Cage Induction Motors Using Combined Park's Vector and Extended Park's Vector Approaches. *Electronics* **2022**, *11*, 380. [CrossRef]
35. Hamani, K.; Kuchar, M.; Kubatko, M.; Kirschner, S. Advancements in Induction Motor Fault Diagnosis and Condition Monitoring: A Comprehensive Review. *Sensors* **2025**, *25*, 5942. [CrossRef] [PubMed]
36. Barrera-Llanga, K.; Burriel-Valencia, J.; Sapena-Bañó, Á.; Martínez-Román, J. A Comparative Analysis of Deep Learning Convolutional Neural Network Architectures for Fault Diagnosis of Broken Rotor Bars in Induction Motors. *Sensors* **2023**, *23*, 8196. [CrossRef] [PubMed]
37. Yang, Y.; Haque, M.M.M.; Bai, D.; Tang, W. Fault Diagnosis of Electric Motors Using Deep Learning Algorithms and Its Application: A Review. *Energies* **2021**, *14*, 7017. [CrossRef]
38. Ibrahim, A.; Anayi, F.; Packianather, M.; Alomari, O.A. New Hybrid Invasive Weed Optimization and Machine Learning Approach for Fault Detection. *Energies* **2022**, *15*, 1488. [CrossRef]
39. Kawady, T.A.; Khater, W.M.; Abu-Faty, H.G.; Izzularab, M.A.; Ibrahim, M.E. AI driven fault diagnosis approach for stator turn to turn faults in induction motors. *Sci. Rep.* **2025**, *15*, 20125. [CrossRef] [PubMed]
40. Ali, A.; Kamal, K. Robust Fault Detection in Industrial Machines Using Hybrid Transformer-DNN with Visualization via a Humanoid-Based Telepresence Robot. *IEEE Access* **2025**, *13*, 115558–115580. [CrossRef]
41. Penman, J.; Sedding, H.; Lloyd, B.; Fink, W. Detection and location of interturn short circuits in the stator windings of operating motors. *IEEE Trans. Energy Convers.* **1994**, *9*, 652–658. [CrossRef]